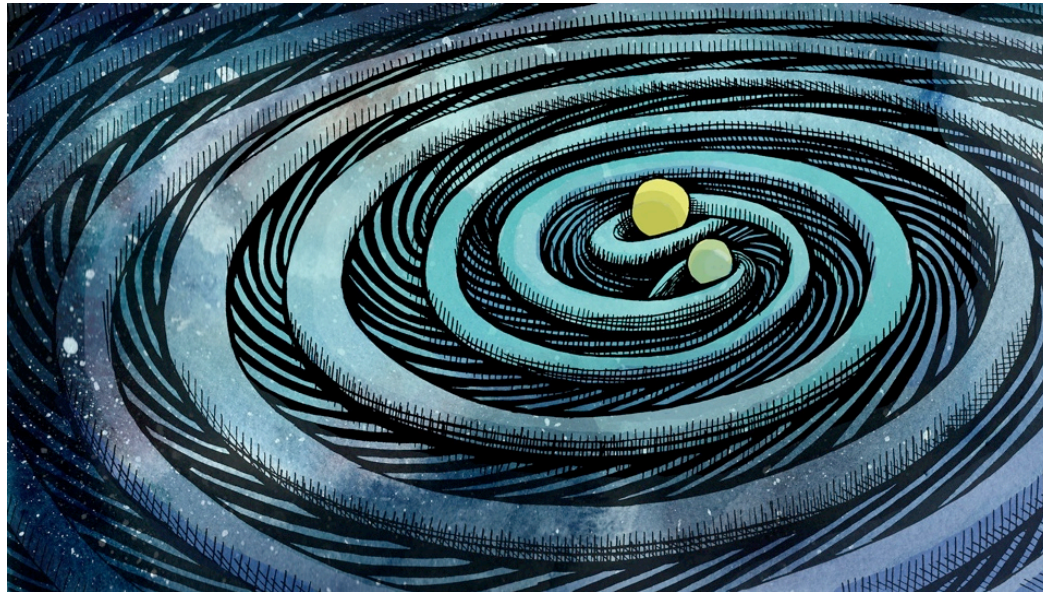


# Numerical-relativity modelling of astrophysical sources of gravitational waves



José Antonio Font  
Universitat de València  
[www.uv.es/virgogroup](http://www.uv.es/virgogroup)



# Outline

Lecture 1: Hydrodynamics and MHD

Lecture 2: Einstein's equations

Lecture 3: Numerical methods

Lecture 4: Applications in astrophysics

- Binary neutron star mergers
- Core collapse supernovae

## Lecture 4

### Applications in astrophysics

- Binary neutron star mergers
- Core collapse supernovae

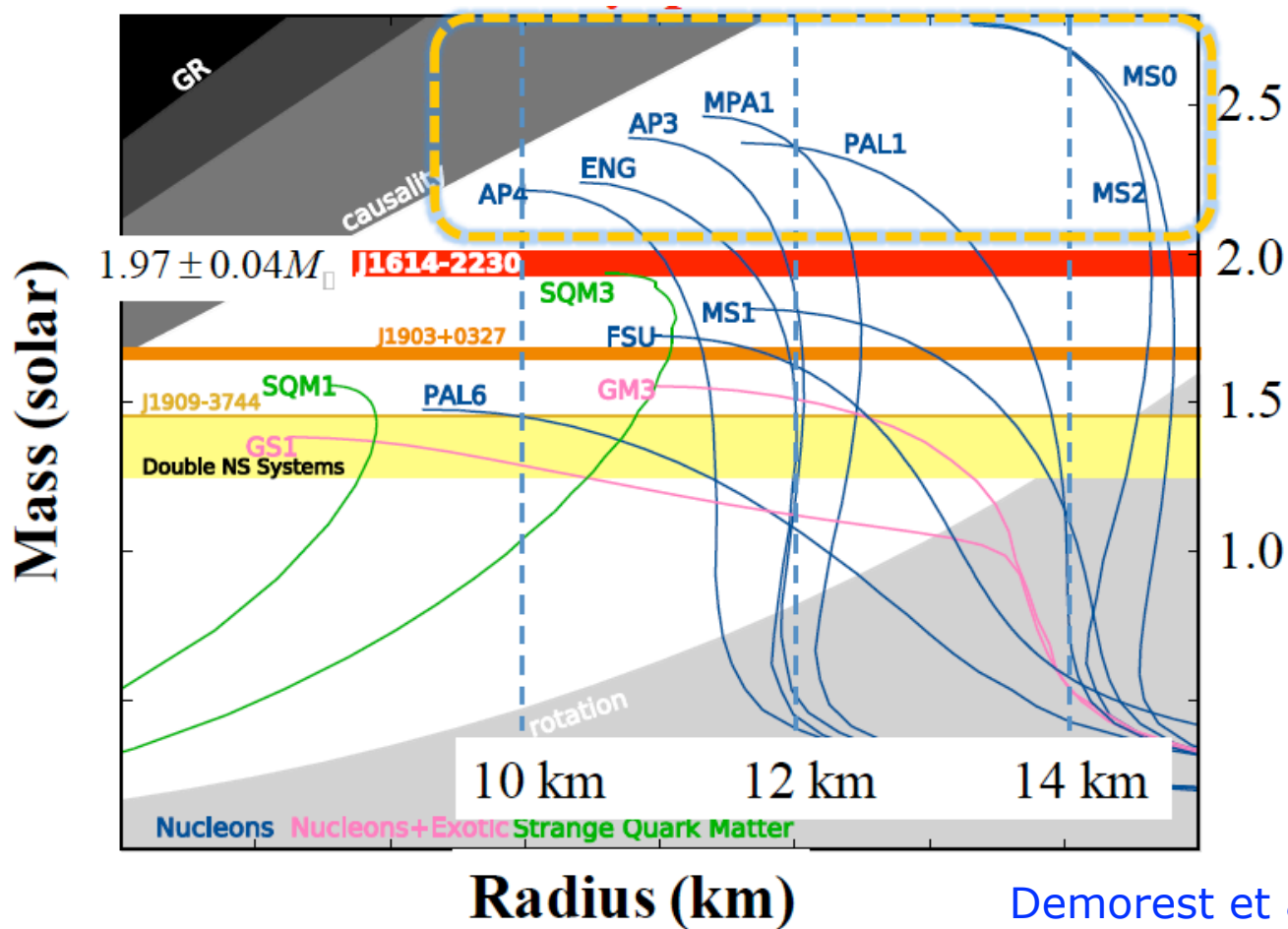
### Asteroseismology of neutron stars with GW observations

De Pietri, Feo, J.A.F., Löffler, Maione, Pasquali, Stergioulas, PRL, **120**, 221101 (2018)

Torres-Forné, Cerdá-Durán, Obergauliner, Müller, J.A.F., PRL, **123**, 051102 (2019)

# Neutron stars

First neutron star detected about 50 years ago. Still, the fundamental properties of matter in the core of neutron stars remain largely uncertain. **No accurate radius** determination.



# Constraints on neutron star radii

The detection of **GWs from NS** may provide alternative approaches to those from the EM spectrum to constrain the properties of NS (mass, radius, EOS):

- **Tidal effects** on gravitational waveforms during inspiral phase of BNS mergers (quadrupole tidal deformability).
- **Oscillations** in post-merger phase of **BNS mergers**.
- **Oscillations** in post-bounce phase of **core-collapse supernovae**.

During LIGO/Virgo **O3** run (started on April 1st 2019), the number of BNS detections is expected to increase. 2 candidates already!

Important to develop improved phenomenological waveform templates (including precession, tides, etc) for the **inspiral phase** (PN theory, EOB).

- Yields information on the EOS, masses and radii from the tidal deformability parameter ([LVC, 1710.05832](#), [1805.11579](#), [1805.11581](#)).

# EOS from inspiral signal

[Read+ \(2013\)](#): systematic investigation of inspiral using extended set of EOS and multiple codes. Last part of inspiral signal carries imprint of the (dimensionless) **quadrupole tidal deformability**  $\Lambda$ .

$$\Lambda = \frac{2}{3} k_2 \left( \frac{R}{M} \right)^5 \quad \begin{array}{l} k_2 \text{ quadrupole} \\ \text{Love number} \end{array}$$

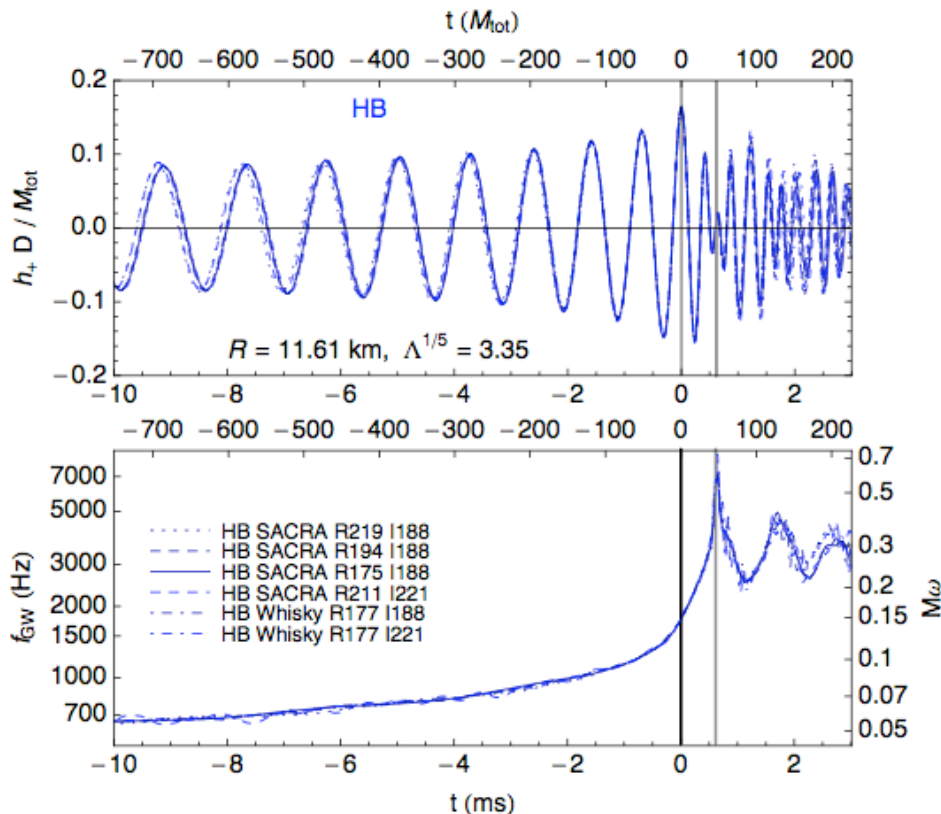
Expected measurability of  $\Lambda$  in 2G and 3G GW detectors.

Using numerical waveforms, two EOS which vary in radius by 1.3 km are distinguishable in mergers at 100 Mpc.

Advanced LIGO/Virgo  $\Delta R/R \sim 10\%$

@ 100 Mpc

[Hotokezaka+ \(2016\)](#): more EOS, better ID (less eccentric), longer inspirals, and lower frequencies ( $\sim 30$  Hz): same estimate up to 200 Mpc.

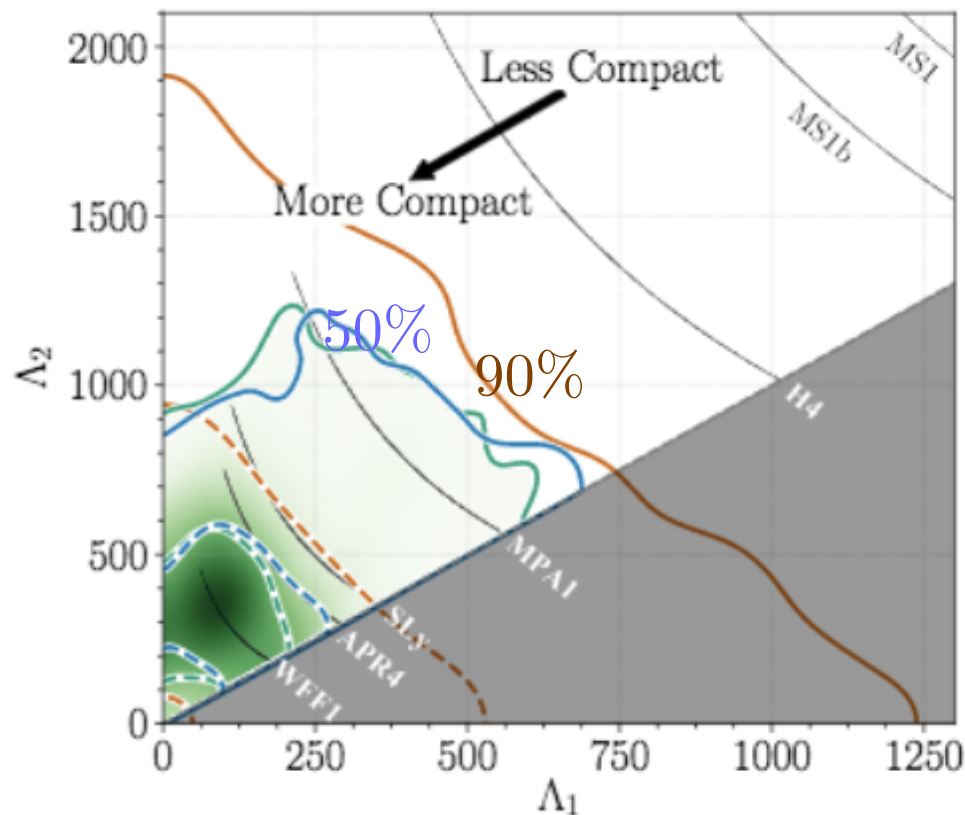


# GW170817: constraints on the NS EOS

Gravitational waves contain information about NS tidal deformations

- allows to constraint NS equation of state (EOS)
- becomes significant above  $f_{\text{GW}} \approx 600$  Hz

Probability density for  $\Lambda_1, \Lambda_2$



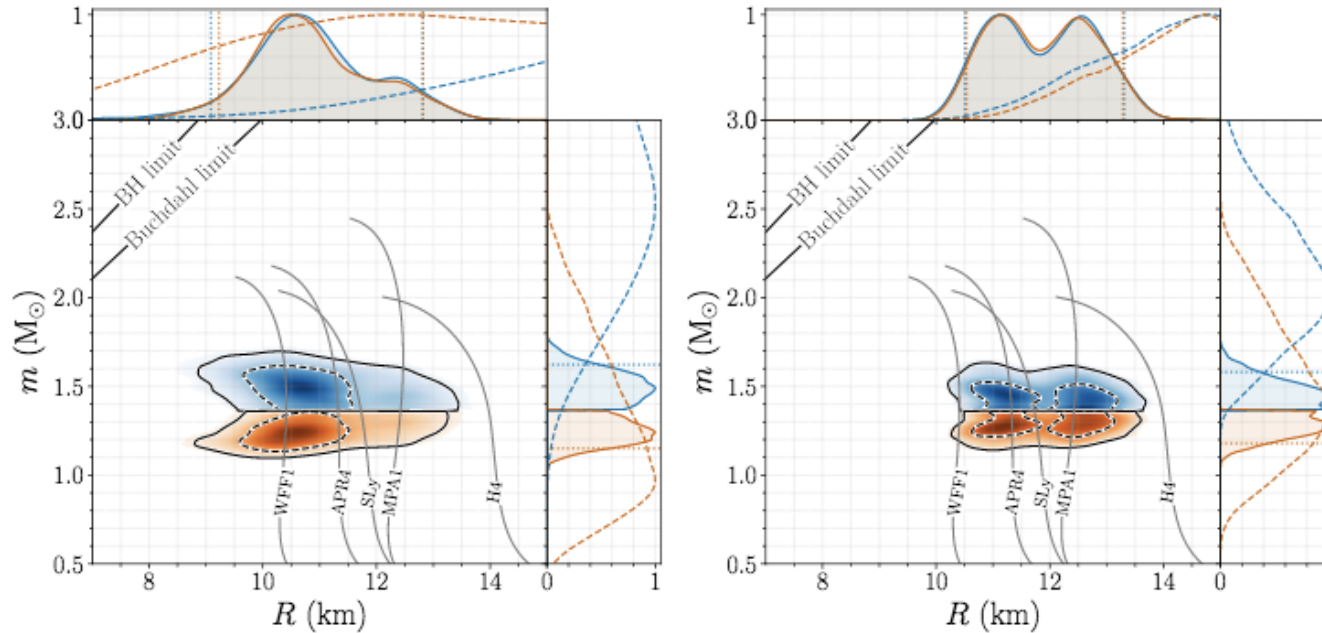
[LVC 1805.11581](#)

“Soft” EOS (more compact NS), such as APR4 or SLy, which predict smaller values of  $\Lambda$ , are favored over “stiff” EOS (less compact NS), such as H4 or MS1, which lie outside the 90% credible region.

**GW170817 data consistent with soft EOS and more compact NS.**

# GW170817: constraints on NS radii

Marginalized posterior for mass  $m$  and areal radius  $R$  (LVC 1805.11581)



Assumption: both NS described by same EOS and have spins within the range observed in Galactic BNS.

(Left) EOS-insensitive relations between various macroscopic properties of the NSs. (Right) a parameterization of the EOS function  $p(\rho)$ .

$$R_1 = 10.8^{+2.0}_{-1.7} \text{ km}$$

$$R_2 = 10.7^{+2.1}_{-1.5} \text{ km}$$

90% credible level

$$R_1 = 11.9^{+1.4}_{-1.4} \text{ km}$$

$$R_2 = 11.9^{+1.4}_{-1.4} \text{ km}$$

# Neutron star oscillations

Important to further develop GW templates for the **merger and post-merger phase** from **Numerical Relativity** simulations (Baiotti & Rezzolla 2017, De Pietri+ 2018, Dietrich+ 2018).

- End-product of the merger?
- Oscillation modes of neutron stars

Equally important to further develop GW templates for the **post-bounce oscillations of PNS in CCSNe**.

- Oscillation modes of neutron stars

This lecture focuses on the information of NS properties that can be inferred from the analysis of the **oscillation spectrum** of NS in the context of **BNS mergers** and **CCSNe**.

# Neutron star oscillations

Interiors of pulsating stars can be investigated through the analysis of their **pulsation modes**. Modes characterized by the nature of the **restoring force** responsible for the oscillatory behavior.

Expansion of the Lagrangian displacement (linear perturbation):

$$\xi(r, \theta, \phi) = \sum_{l=0}^{\infty} \sum_{m=-l}^l [U_l^m(r) Y_l^m(\theta, \phi) \hat{e}_r + V_l^m(r) \nabla Y_l^m(\theta, \phi) + W_l^m(r) \hat{e}_r \times \nabla Y_l^m(\theta, \phi)]$$

Main oscillation modes:

1. *f*-modes / *p*-modes

fluid modes restored by pressure

2. *g*-modes

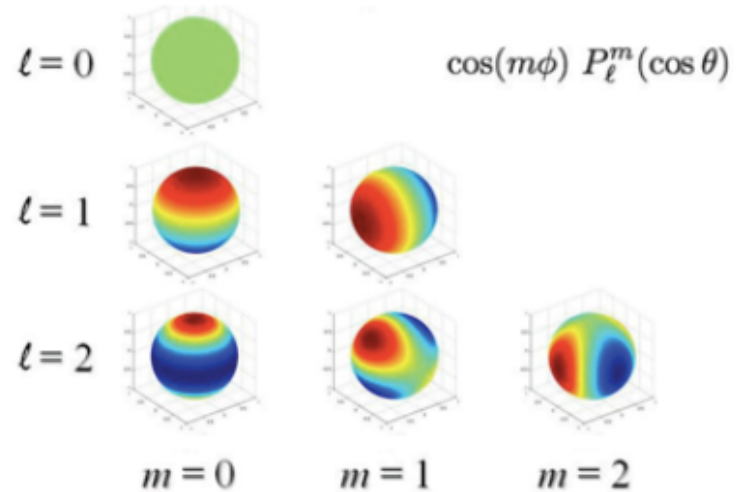
restored by gravity/buoyancy

3. inertial modes (*r*-modes)

restored by the Coriolis force in *rotating* stars

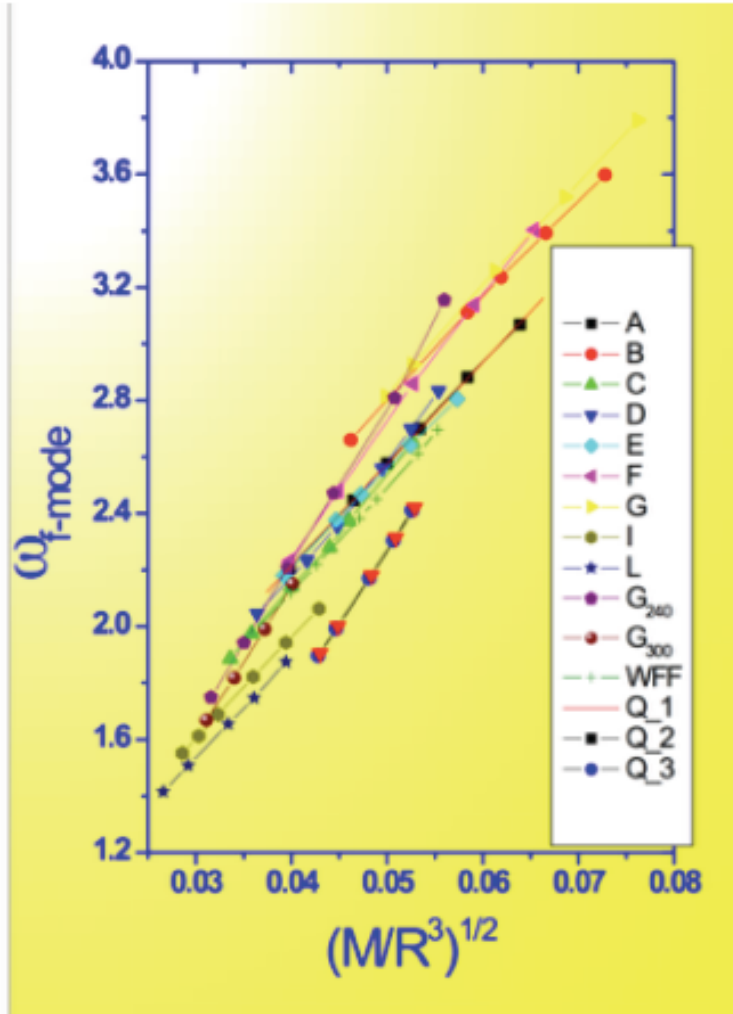
4. *w*-modes

*spacetime* modes (similar to black hole modes)



Friedman &  
Stergioulas (2013)

# GW asteroseismology



Andersson & Kokkotas (1998)

Eigenfrequencies of most important modes of **pulsating NS**: fundamental fluid **f-mode**, first pressure **p-mode** and first **w-mode**, for 12 realistic EOS.

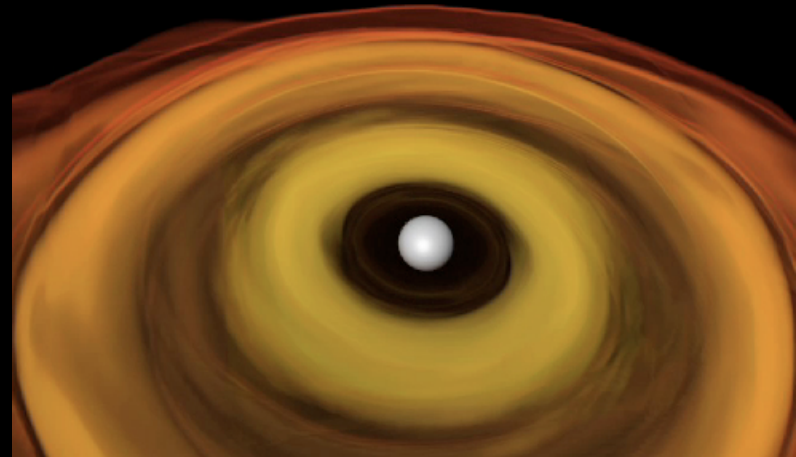
Robust **empirical relations** between mode-frequencies and NS parameters ( $R$  and  $M$ ) inferred from the data. Can be used to extract the details of the star from observed modes (inversion problem).

If pulsation modes of NS are observed by GW detectors, the mass and radius of NS could be deduced within a few % error.

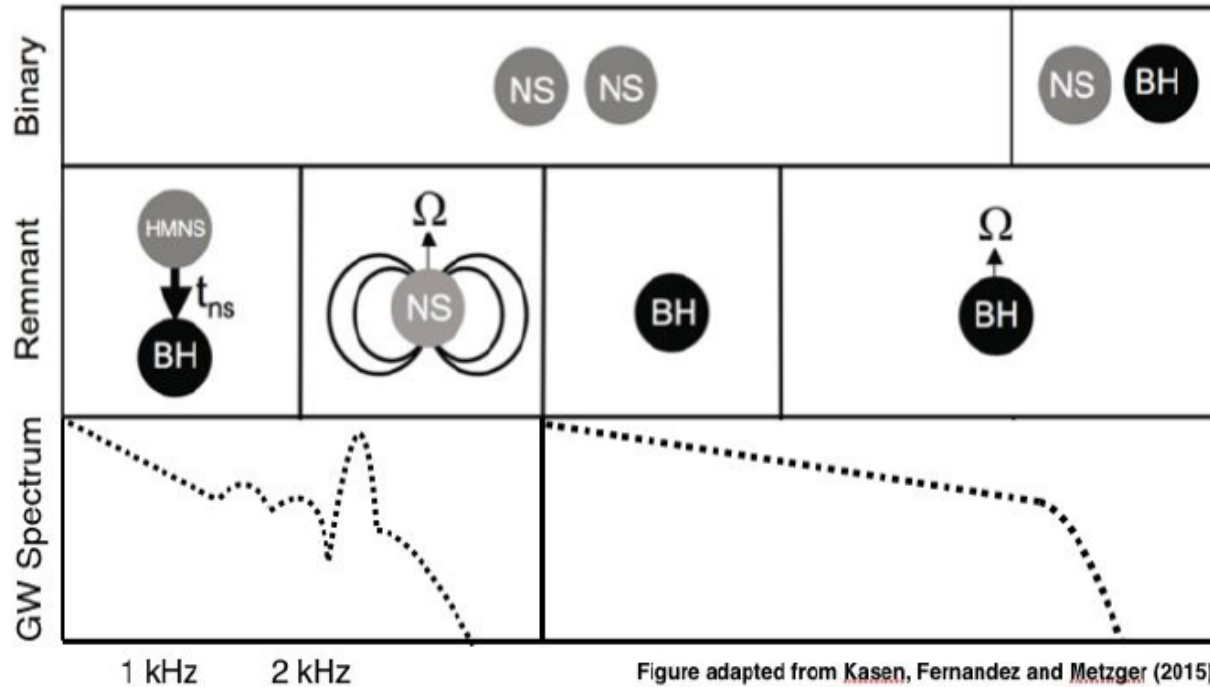
$$\omega_f(\text{kHz}) \approx 0.78 + 1.637 \left( \frac{M}{R^3} \right)^{1/2}$$

# Astrophysical situation #1

Oscillations of "hypermassive" NS



# GWs from BNS post-merger remnant



## Possible outcome:

- Prompt collapse (BH ringing  $> 6$  kHz)
- HMNS ( $t_{GW} \sim \text{few-10 ms}$ )
- SMNS ( $t_{GW} \sim 10\text{-}100$  ms)
- Stable remnant ( $t_{GW} \sim 100$  ms, minutes, weeks+)

**HMNS:** "Hypermassive" star. Remnant supported by differential rotation and thermal gradients.

**SMNS:** "Supramassive" star. Mass small enough to be supported by rigid rotation.

# GW170817 - search for post-merger GWs

LIGO-Virgo Collaboration (Abbott+ 2017)

Search for signals of short duration ( $\leq 1$  s) (cWB; Klimentenko+ 2016) and intermediate duration ( $\leq 500$ s) (STAMP Thrane+ 2011 y cWB) in the LIGO/Virgo data, including emission from HMNS or SMNS, respectively.

**No GW signal from post-merger remnant found.**

Upper limits (root-sum-square) of the amplitude, between 1-4 kHz, at a 50% detection efficiency

Short signal: 
$$h_{\text{rss}}^{50\%} = 2.1 \times 10^{-22} \text{ Hz}^{-1/2}$$

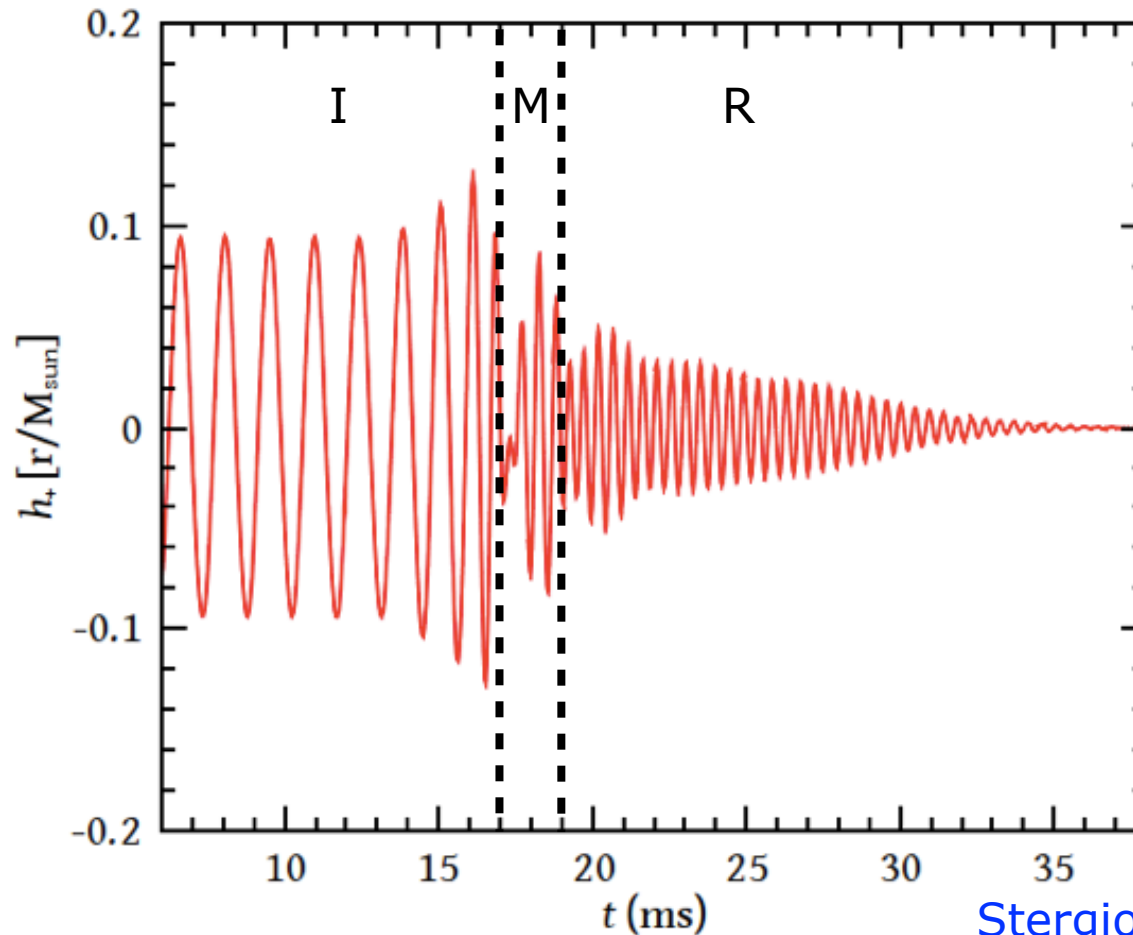
Intermediate signal: 
$$h_{\text{rss}}^{50\%} = 8.4 \times 10^{-22} \text{ Hz}^{-1/2} \quad (\text{ms magnetar model})$$

$$h_{\text{rss}}^{50\%} = 5.9 \times 10^{-22} \text{ Hz}^{-1/2} \quad (\text{bar-mode model})$$

**Post-merger emission** from a GW170817-like event may be detected when LIGO/Virgo reach design sensitivity (a factor 3 improvement with respect to O2) or with **next-generation detectors** (ET, CE).

# Post-merger gravitational waves

The BNS merger GW signal can be divided into three distinct parts: **inspiral** (I), **merger** (M) and post-merger **ringdown** (R).

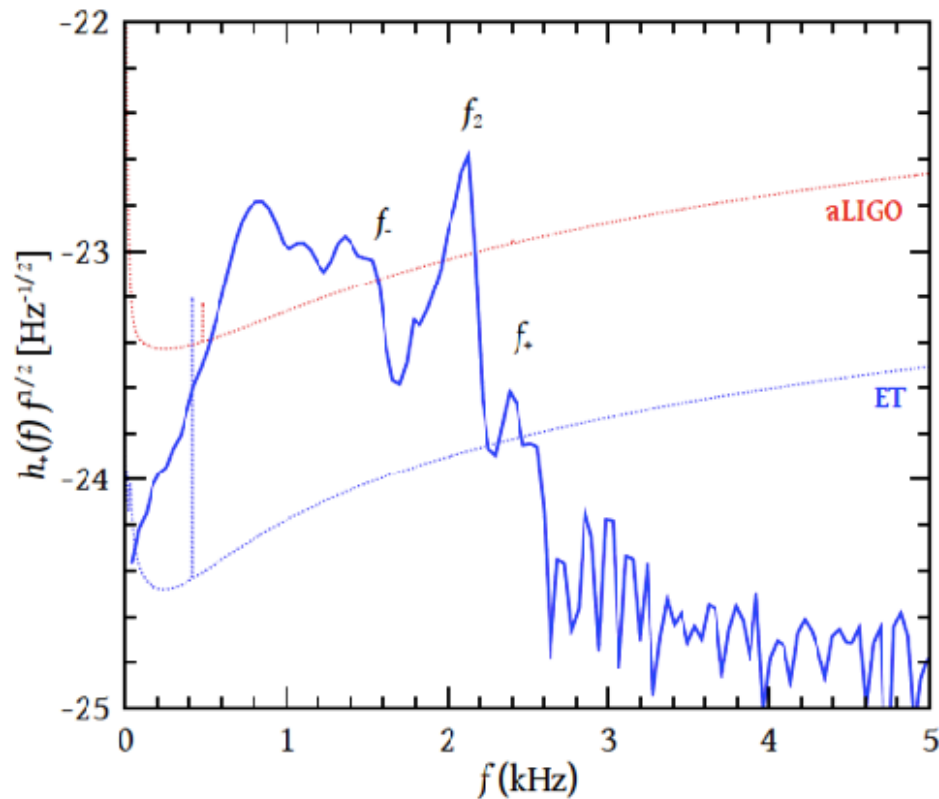


Stergioulas+ (2011)

# Post-merger GW spectrum

**Several peaks** stand above the Advanced LIGO/Virgo or ET sensitivity curves and are **potentially detectable** (Hotokezaka+2011, Stergioulas+2011, Takami+ 2014).

The dominant  $m=2$  f-mode forms a **triplet** with two additional components. **How are these produced?** Mode coupling?

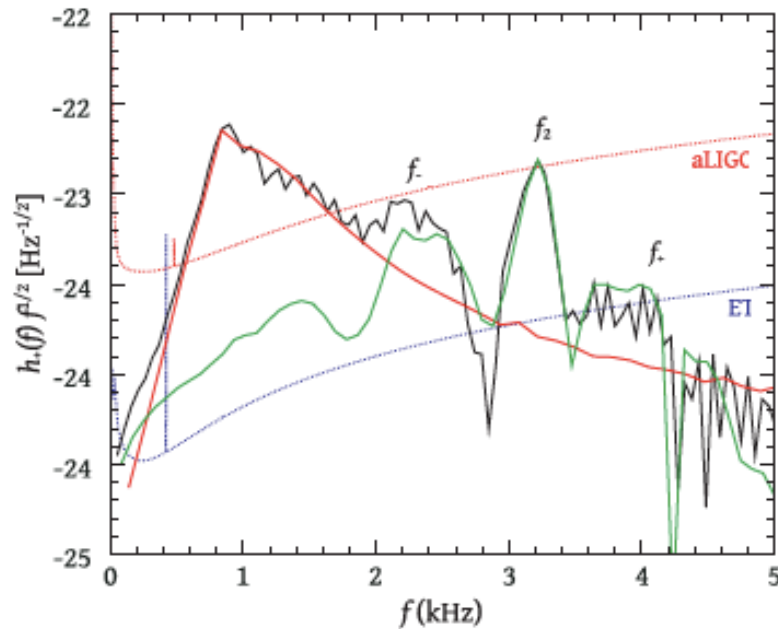


Stergioulas+  
(2011)

# Post-merger GW spectrum

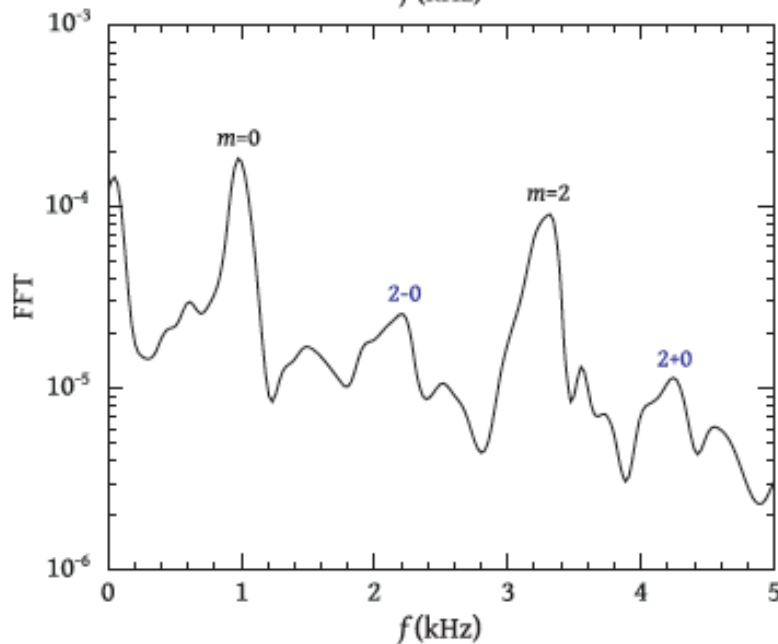
GW spectrum.  
(FFT of GW strain)

total  
inspiral  
post-merger



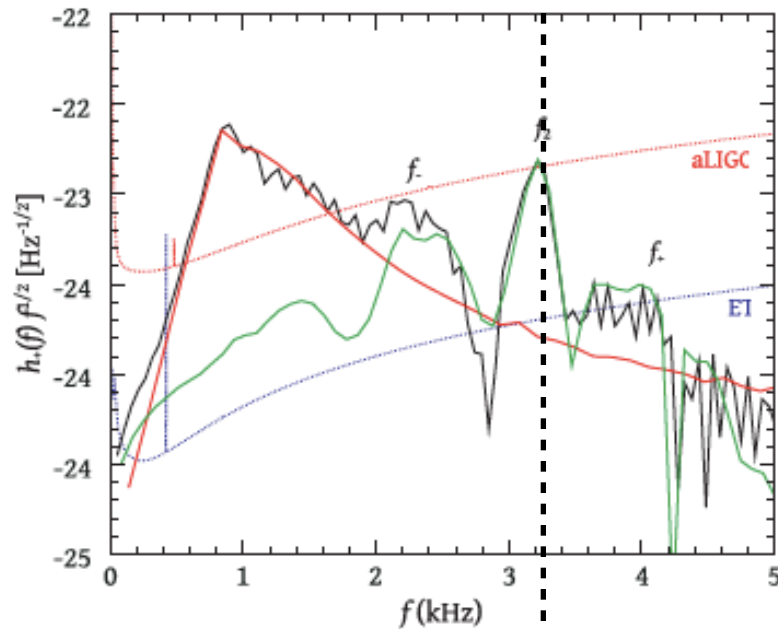
LS 220 EOS  
1.35+1.35

Fourier transform  
of hydrodynamics  
in equatorial plane.



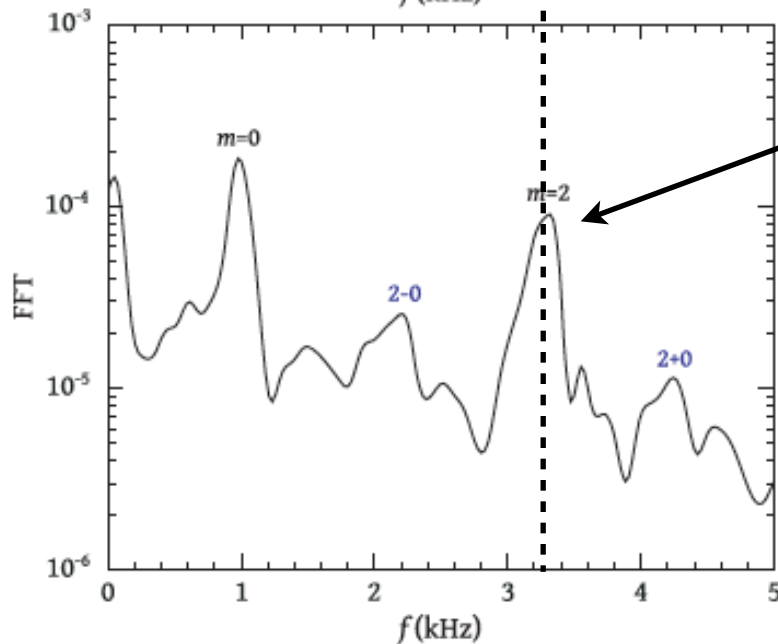
# Post-merger GW spectrum

GW spectrum.  
(FFT of GW strain)



LS 220 EOS  
1.35+1.35

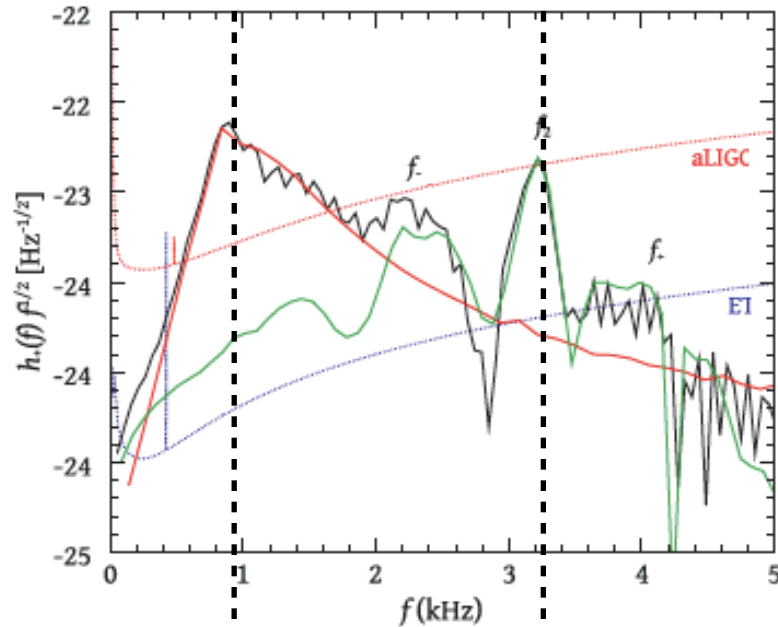
Fourier transform  
of hydrodynamics  
in equatorial plane.



$l = m = 2$   
linear f-mode

# Post-merger GW spectrum

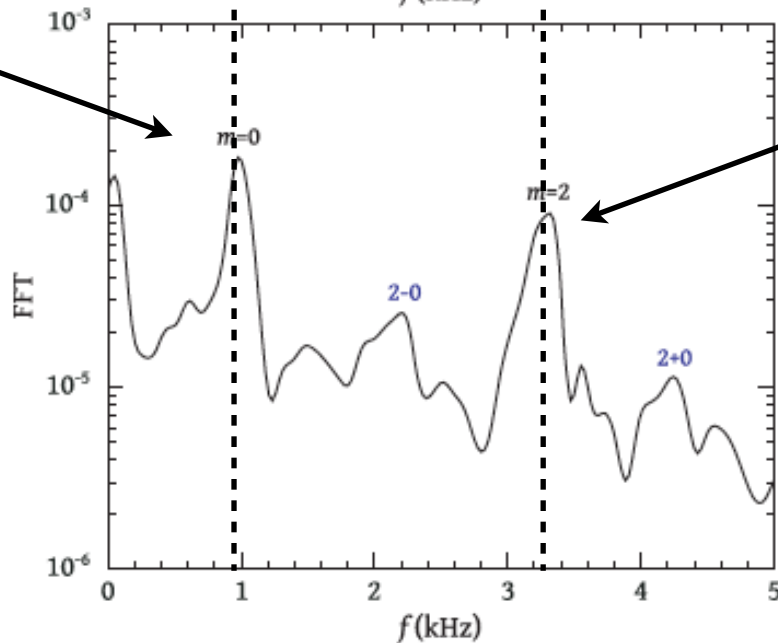
GW spectrum.  
(FFT of GW strain)



LS 220 EOS  
1.35+1.35

$l = m = 0$   
linear quasi-  
radial mode

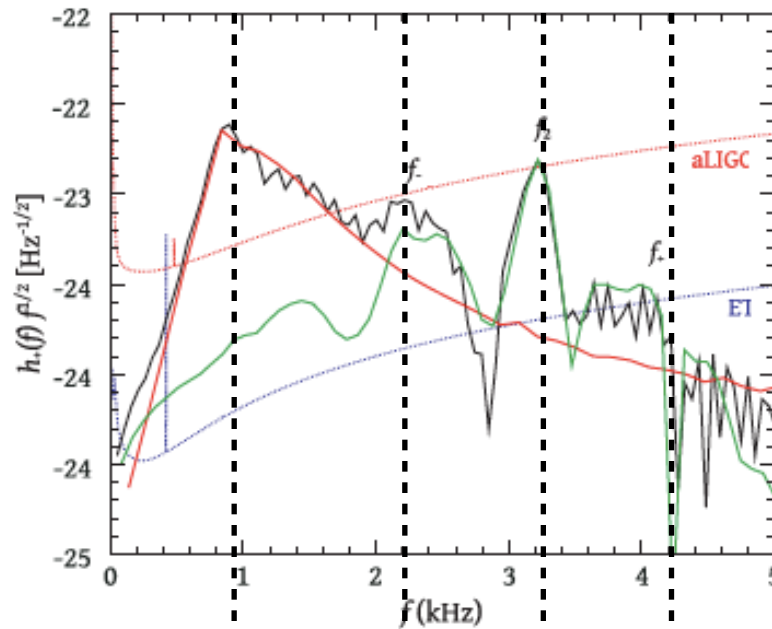
Fourier transform  
of hydrodynamics  
in equatorial plane.



$l = m = 2$   
linear f-mode

# Post-merger GW spectrum

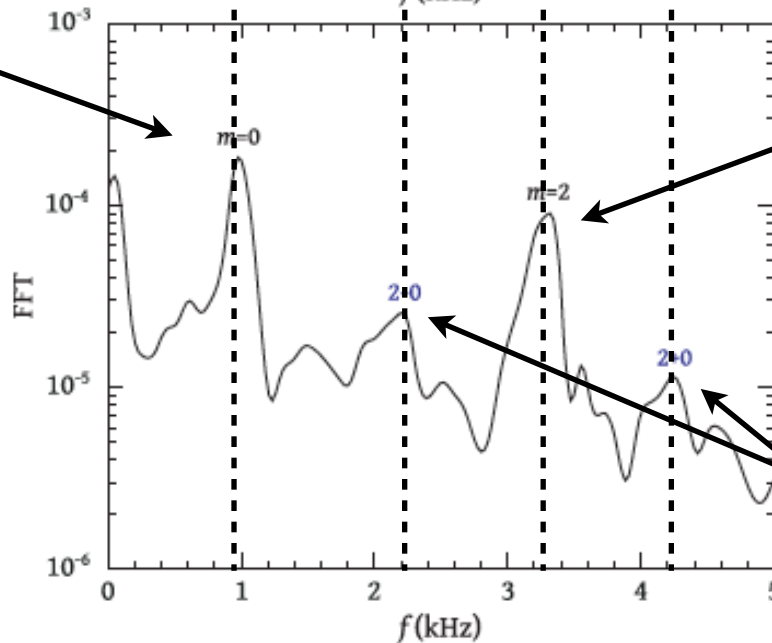
GW spectrum.  
(FFT of GW strain)



LS 220 EOS  
1.35+1.35

$l = m = 0$   
linear quasi-  
radial mode

Fourier transform  
of hydrodynamics  
in equatorial plane.

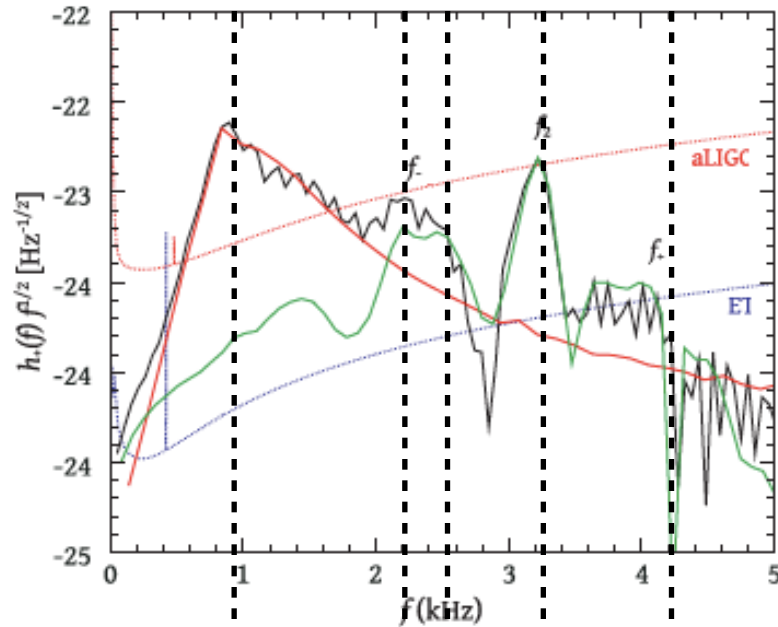


$l = m = 2$   
linear f-mode

"2-0" & "2+0"  
quasi-linear  
combination  
frequencies

# Post-merger GW spectrum

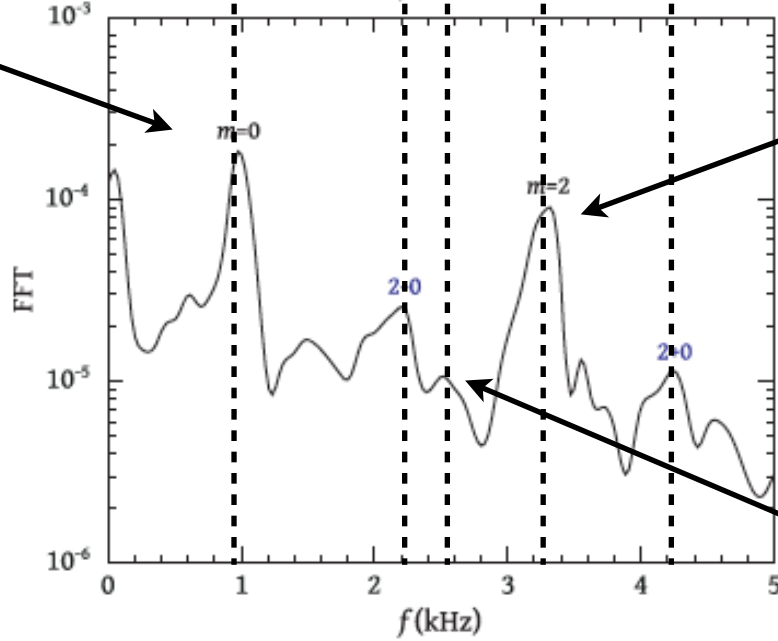
GW spectrum.  
(FFT of GW strain)



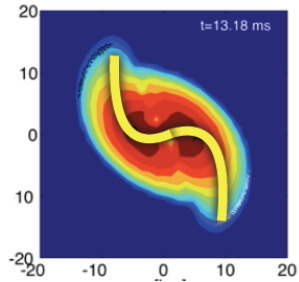
LS 220 EOS  
1.35+1.35

$l = m = 0$   
linear quasi-radial mode

Fourier transform of hydrodynamics in equatorial plane.

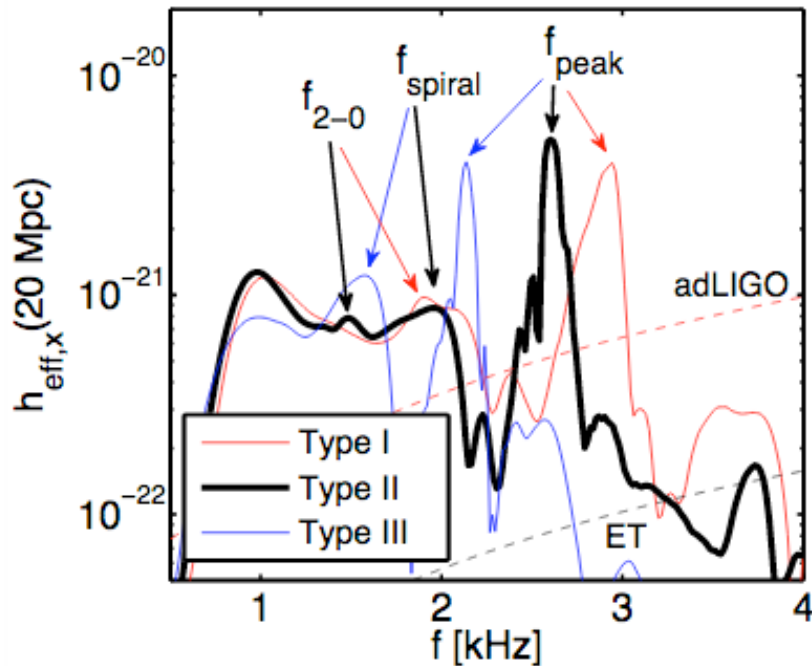
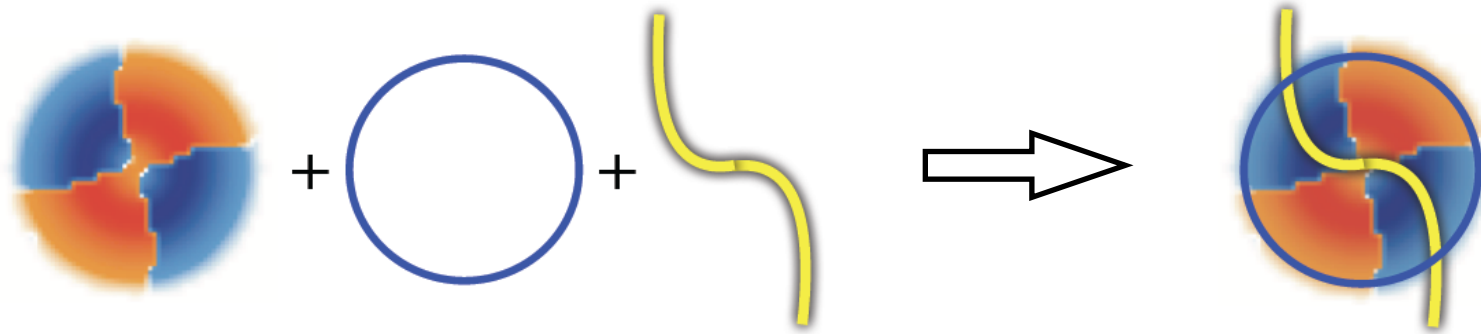


$l = m = 2$   
linear f-mode



non-linear spiral frequency

# Linear + quasi-linear + nonlinear



Type I: "2-0" combination freq. dominates (soft EOS, high mass).

Type II: "2-0" and spiral freqs. present.

Type III: spiral freq. dominates (stiff EOS, low mass).

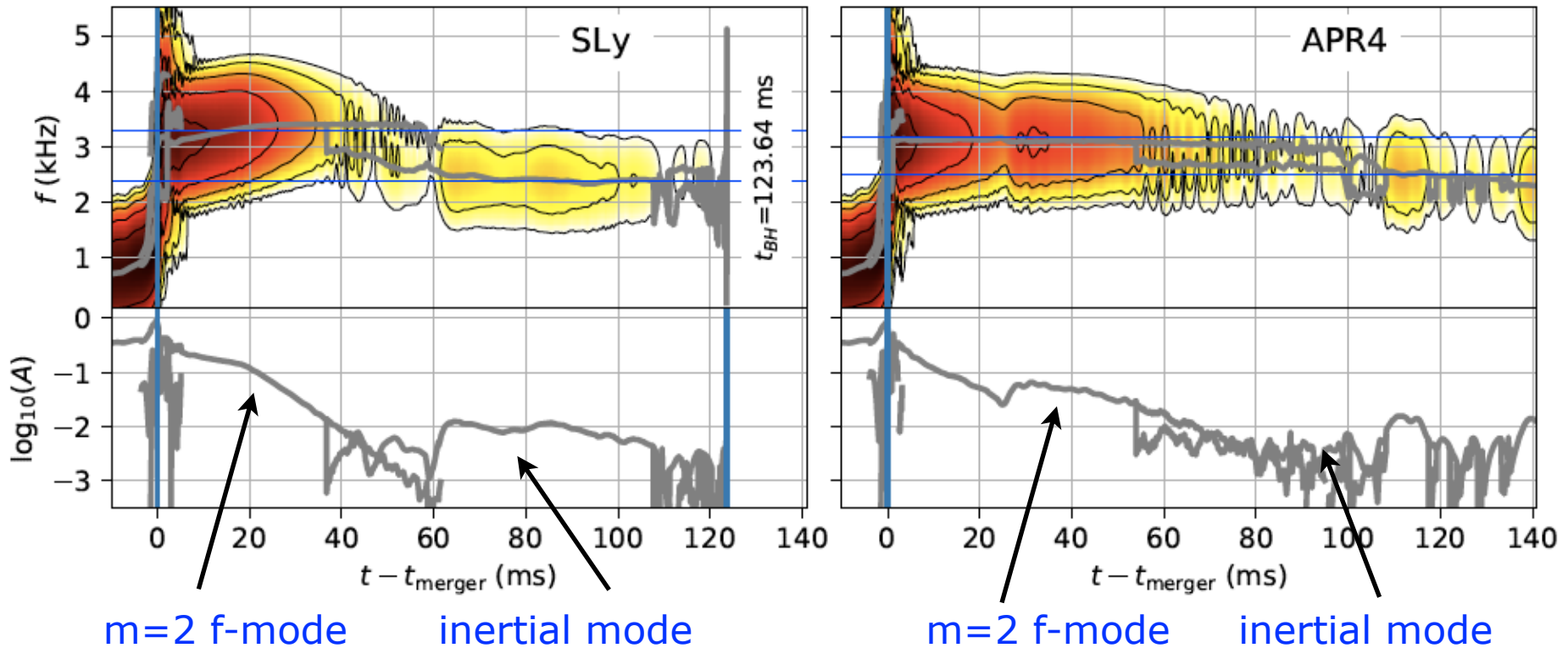
If these observations become available, both the  $m=2$  and  $m=0$  mode frequencies could be extracted.

That would allow for GW asteroseismology of post-merger remnants and would lead to tight **constraints on the EOS**. (Bauswein+ 2014)

Bauswein & Stergioulas (2015)

# Convective excitation of inertial modes

De Pietri+ (2018) have recently performed the longest term simulations of BNS mergers thus far (up to **140 ms** post-merger).



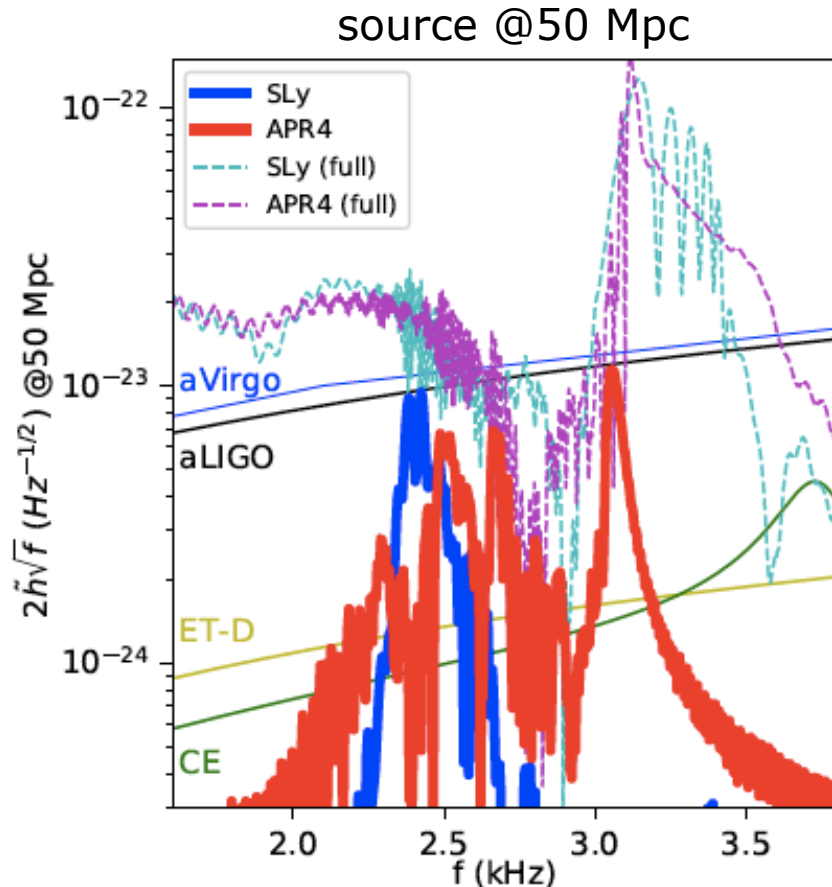
Early post-merger GW emission dominated by the f-mode.

Late post-merger GW emission dominated by a lower-frequency inertial mode (due to convection).

De Pietri+, PRL (2018)

# Late-time GW spectrum

Mode dynamics imprinted in the GW spectrum.



## Full signal:

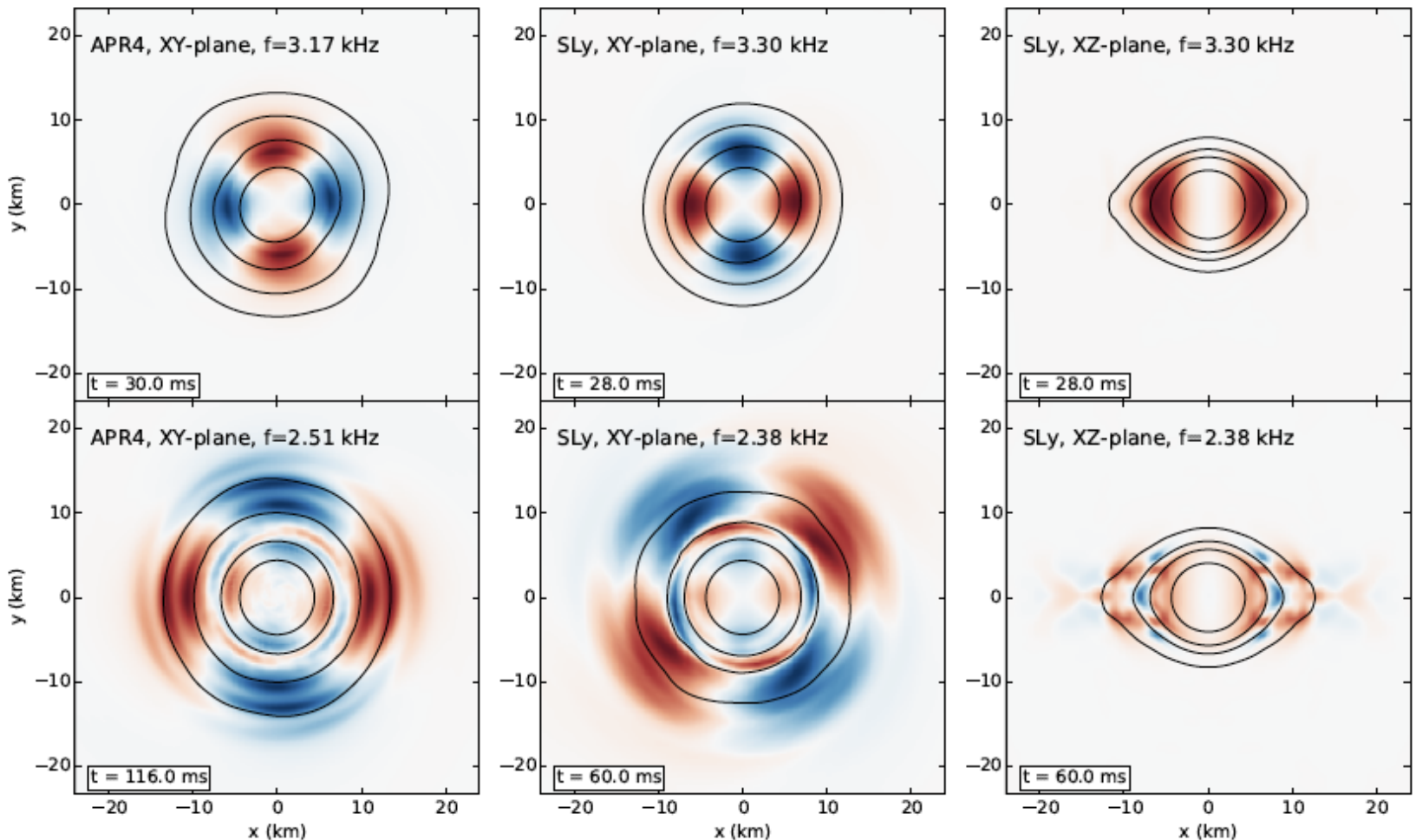
spectrum dominated by the  $f$ -mode ( $>3$  kHz).

## Restricted signal (55-140 ms after merger):

spectrum dominated by lower-frequency inertial modes.

Sufficient power in low-frequency modes to render them potentially observable by 3G detectors.

# Mode (density) eigenfunctions



**Top row:** Early time. No azimuthal nodal line.  $m=2$  f-mode.

**Bottom row:** late time.  $m=2$ . Azimuthal nodal lines (higher radial order modes). Eigenfunction consistent with inertial mode ([Kastaun 2008](#)).

# Convective instability and inertial modes

Growth of inertial modes (up to saturation amplitude) triggered by a **convective instability** that appears in the nonisentropic remnant.

Local convective instability depends on sign of **Schwarzschild discriminant**

$$A_\alpha = \frac{1}{\varepsilon + p} \nabla_\alpha \varepsilon - \frac{1}{\Gamma_1 p} \nabla_\alpha p$$

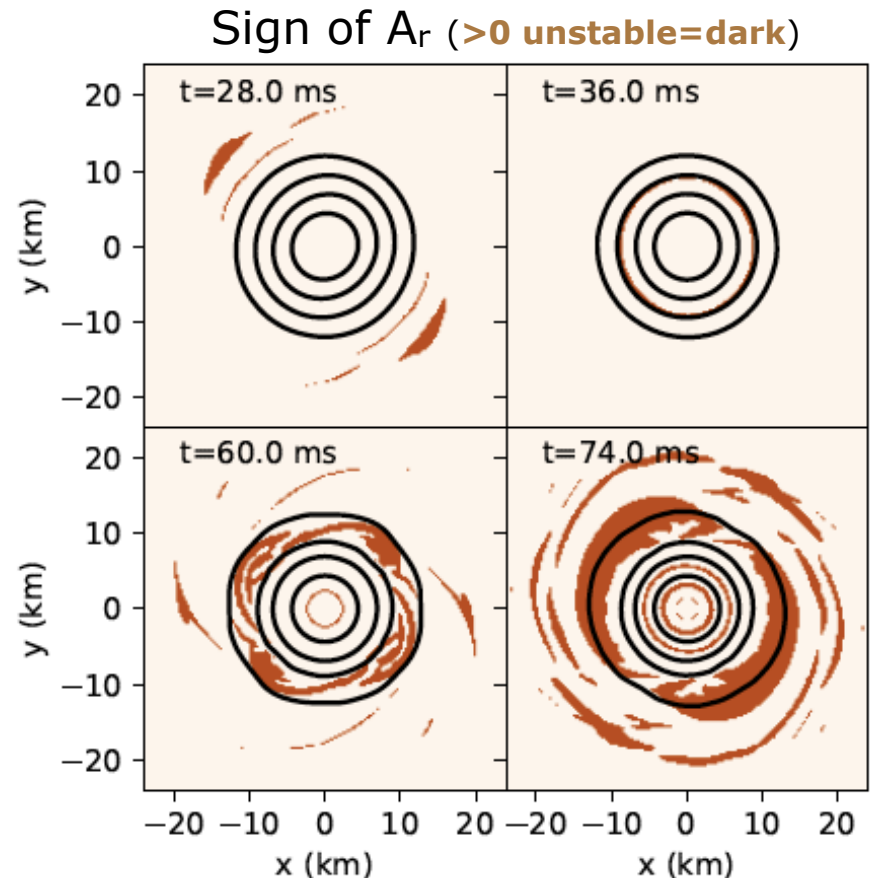
convectively unstable region  $A_\alpha > 0$

$$\Gamma_1 = \Gamma_{\text{th}} + (\Gamma_i - \Gamma_{\text{th}}) \frac{K_i \rho^{\Gamma_i}}{p}$$

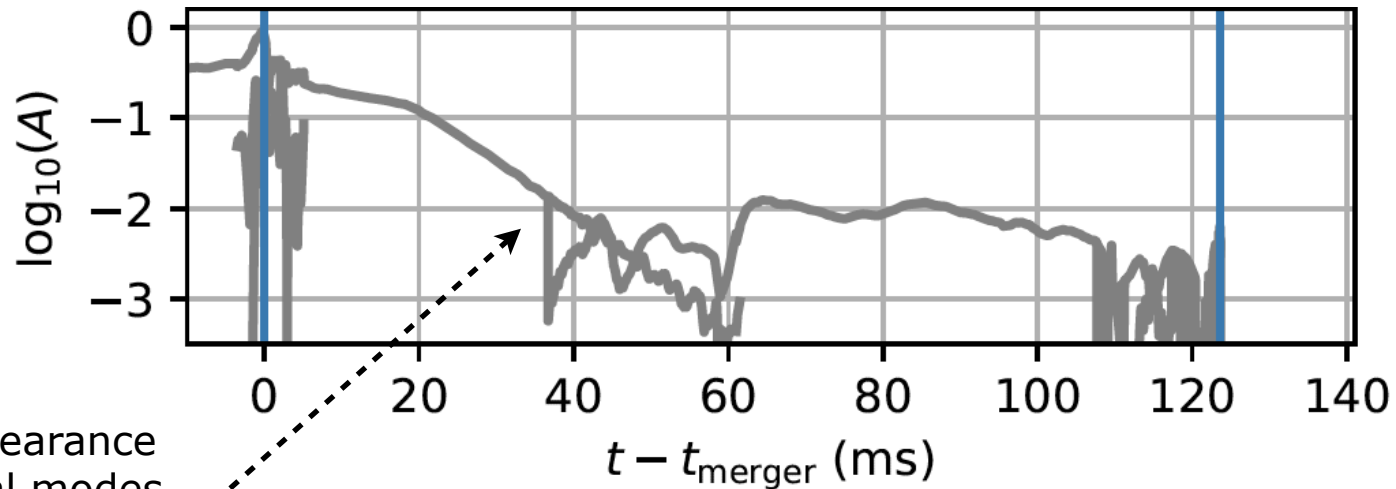
Piecewise polytropic EOS (7 pieces)  
+ thermal part (Read+ 2009 )

About 30-50 ms after merger, parts of the HMNS become **convectively unstable**.

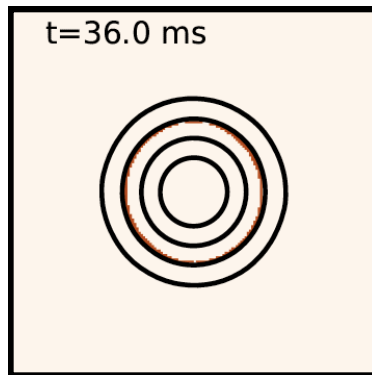
Appearance of convectively unstable regions and growth of inertial modes strongly correlated.



# Convective instability and inertial modes

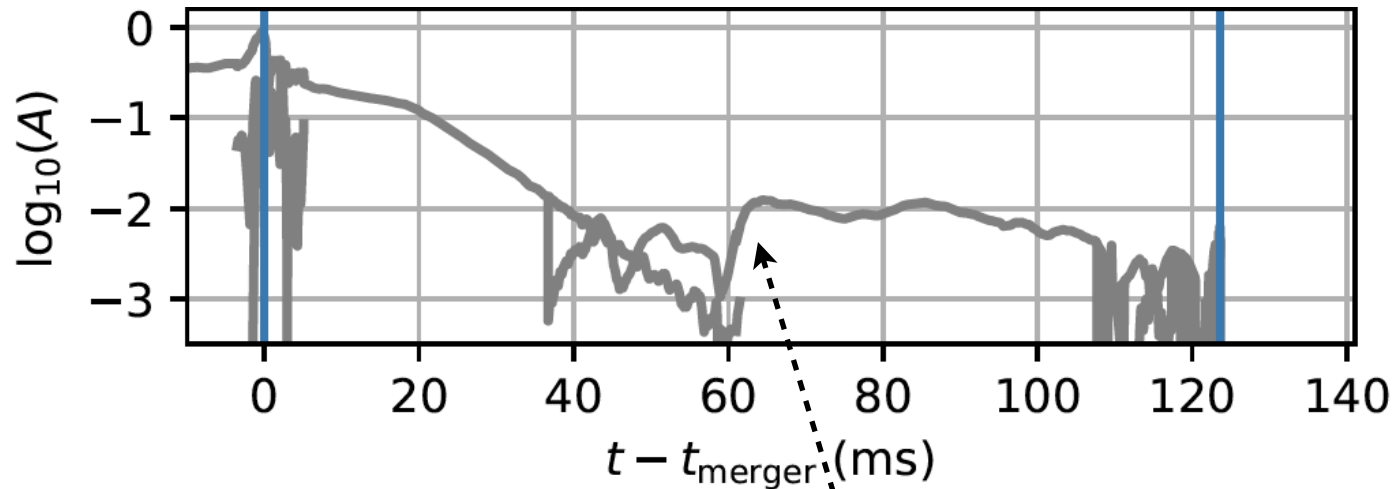


first appearance  
of inertial modes



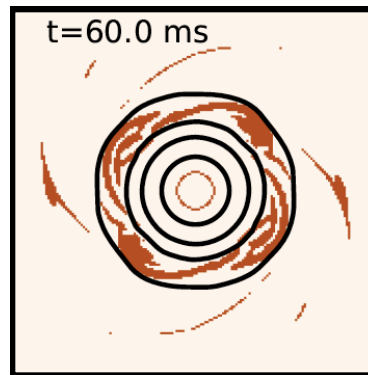
convectively unstable  
ring @ equatorial plane

# Convective instability and inertial modes



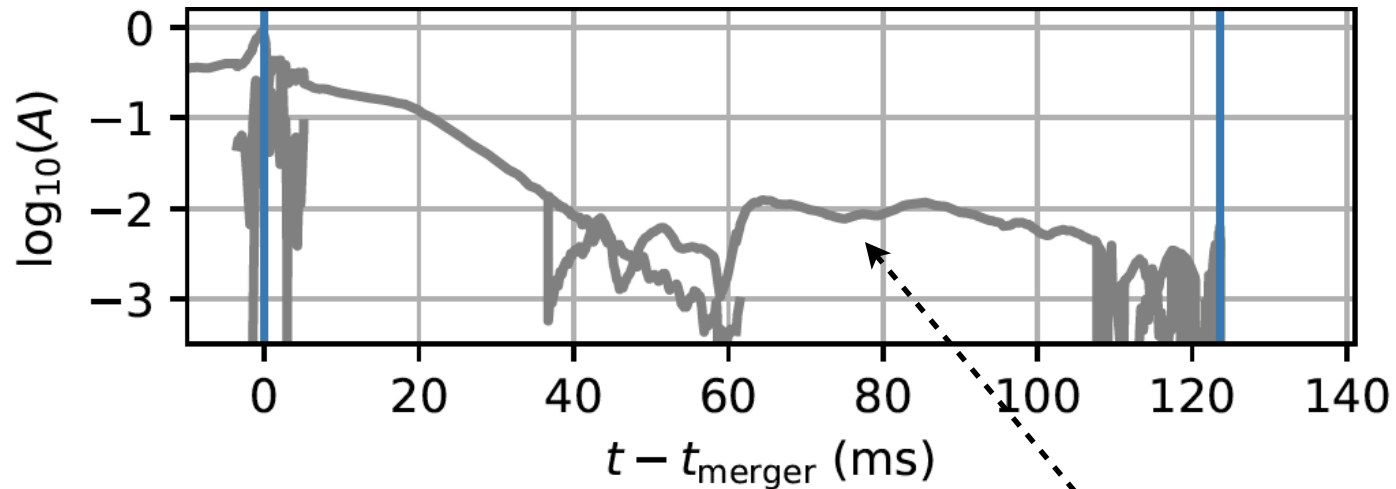
strong growth of  
inertial mode amplitude

$$f = 2.38 \text{ kHz}$$

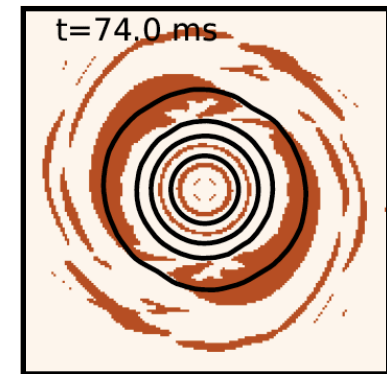


first convectively unstable ring has expanded to  
lower densities and appears fragmented

# Convective instability and inertial modes

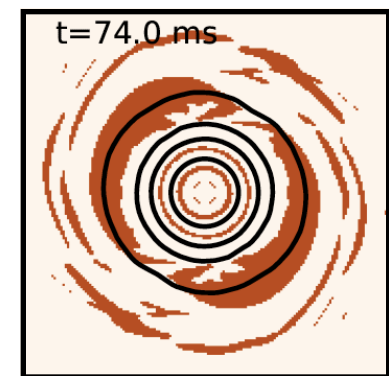
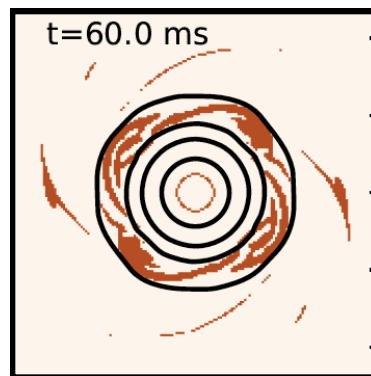
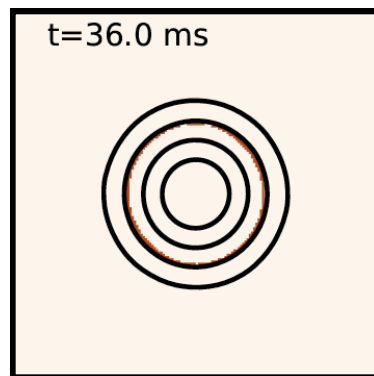
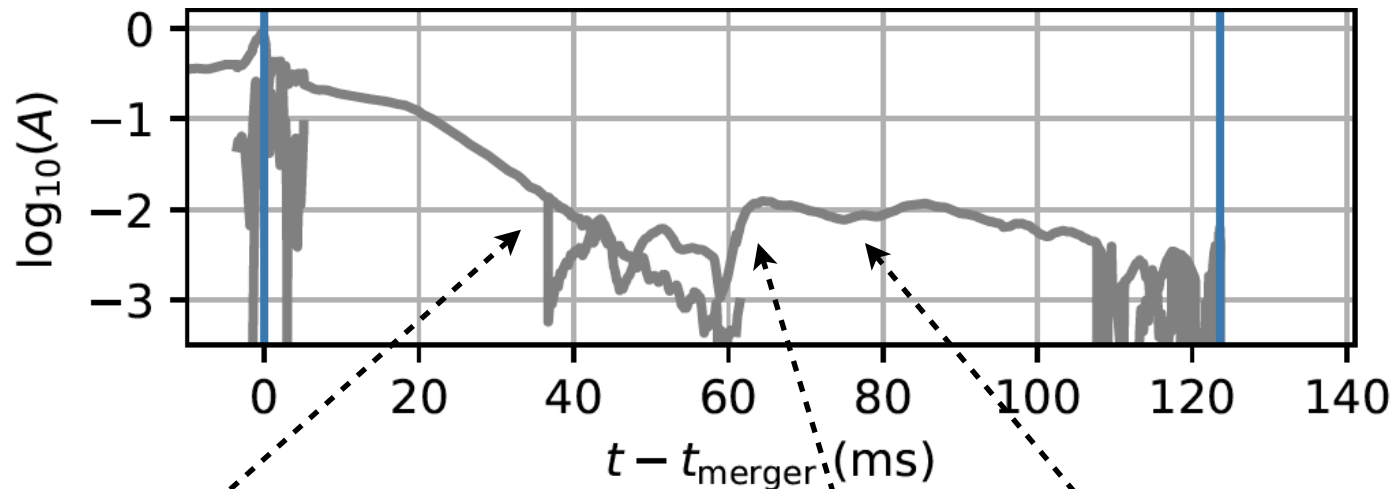


renewed growth of  
inertial mode amplitude



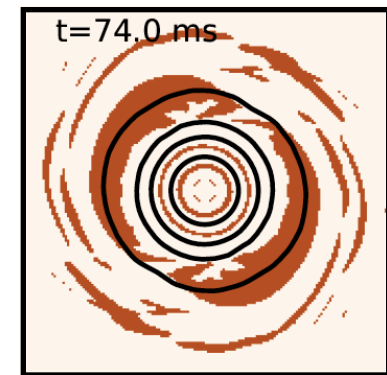
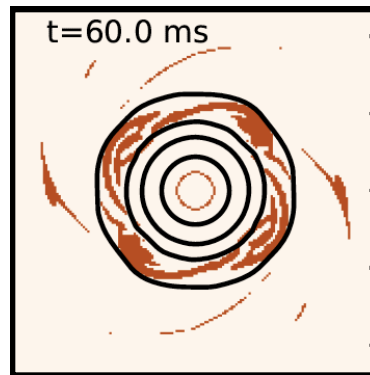
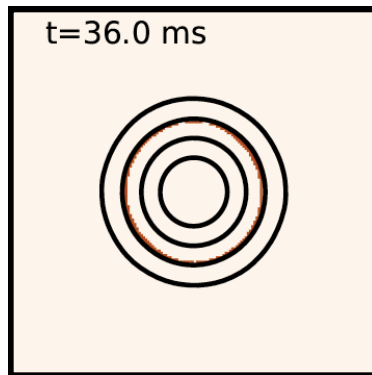
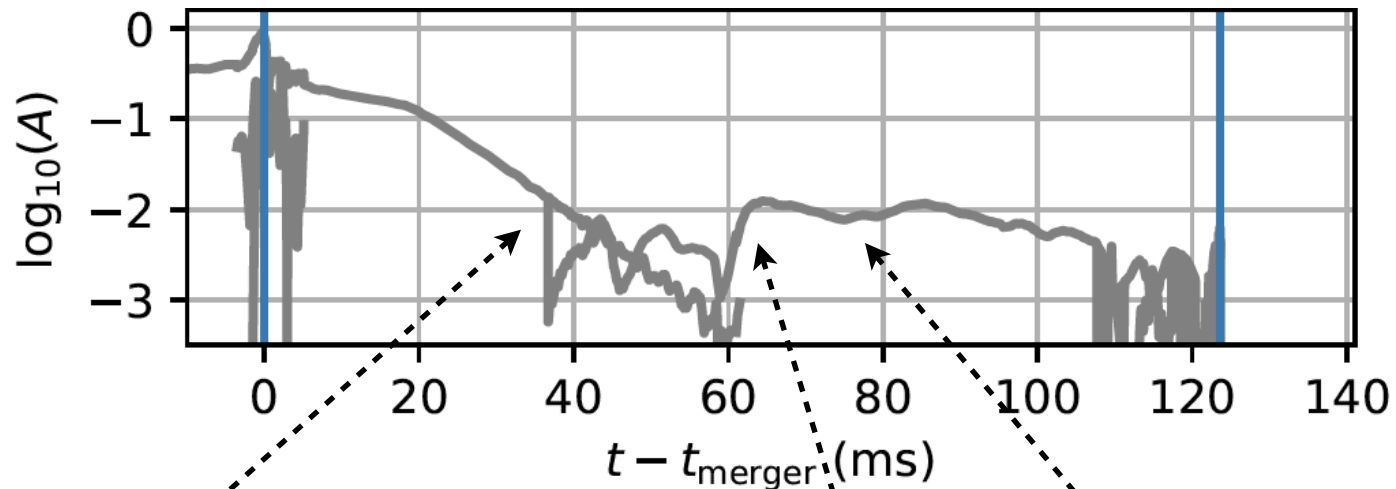
convectively unstable regions  
have expanded further

# Convective instability and inertial modes



Strong correlation between the appearance of convectively unstable regions in the HMNS and the appearance and growth of inertial modes.

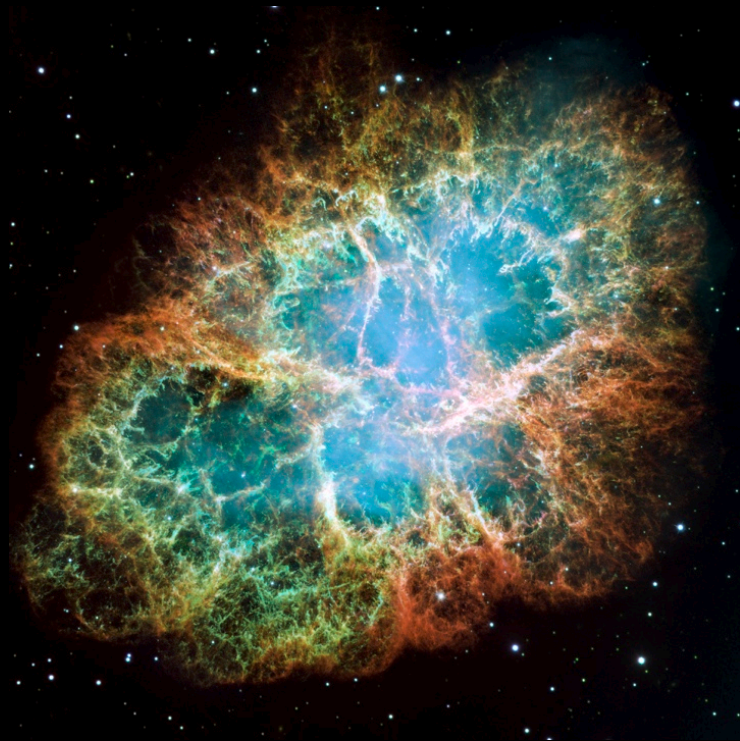
# Convective instability and inertial modes



Since inertial-mode frequencies depend on rotation rate of the star and are triggered by a convective instability, their detection in GWs would **probe the rotational and thermal state of HMNS**.

# Astrophysical situation #2

## Oscillations of PNS in CCSNe



# Looking into the “engine” of a CCSN

Understanding **CCSN** is one of the **primary problems in relativistic astrophysics**.

- **through observations of neutrinos**  
so far only SN1987A
- **through observations of gravitational waves**  
still to be achieved  
would provide a kind of Rosetta stone (as GW170817 for BNS!)
- **through numerical simulations**  
already a 50+ year old effort  
extremely complex and computationally **expensive** 6D radiation-hydrodynamics problem  
~50 million CPU hours / simulation

# Gravitational waves from CCSNe

Einstein quadrupole  
formula

(adequate for CCSN with PNS formation;  
Shibata+ 2005, Reisswig+ 2011)

$$h_{ij} = \frac{2G}{Rc^4} \frac{\partial^2 Q_{ij}}{\partial t^2} \sim \frac{R_S}{R} \frac{v^2}{c^2}$$

$$R_S = 3 \text{ km}, \quad v/c = 0.1, \quad R = 10 \text{ kpc} \quad \rightarrow \quad h \sim 10^{-20}$$

time-dependent mass-energy quadrupole moment in  
CCSN due to

- convection in PNS
- convection in neutrino heated hot bubble
- anisotropic neutrino emission
- any other non-radial instability (e.g. SASI)

**generically produced by any CCSN**

and due to rotation and magnetic fields

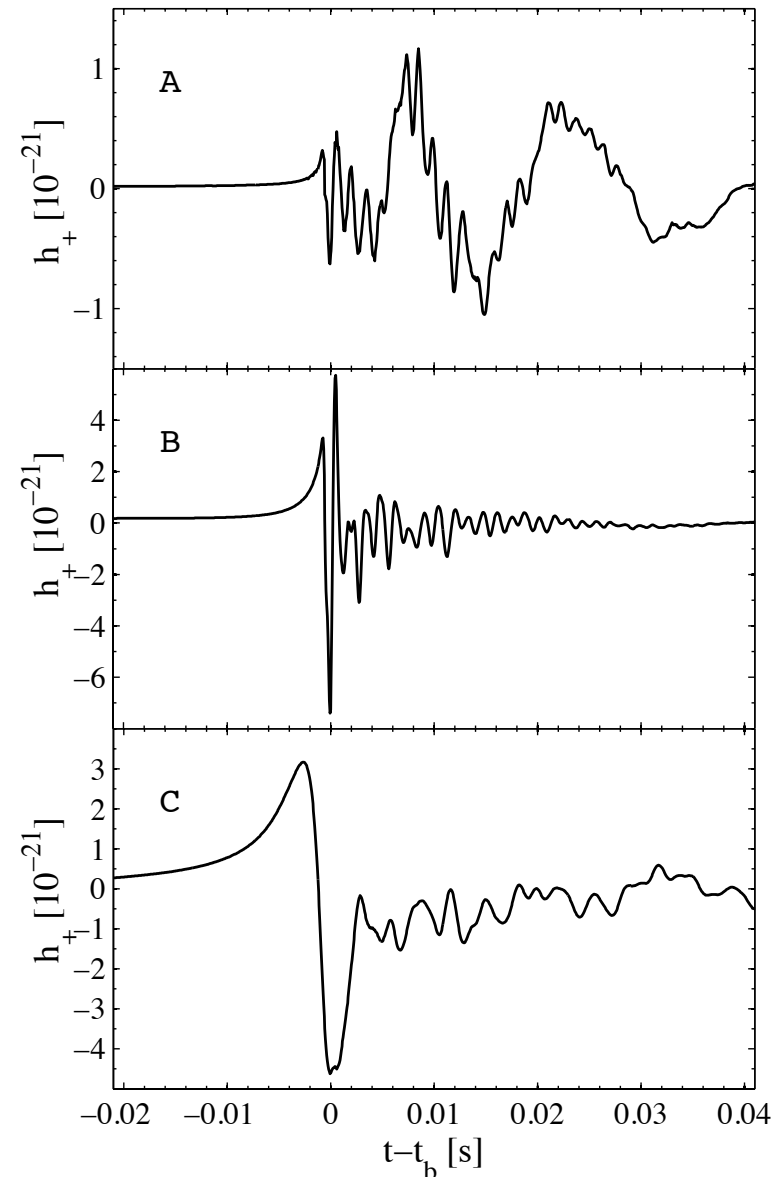
# GW signals at bounce: rotational mechanism

Angular momentum conservation:  
rotating cores with  $P \sim 1$  s produce  
ms period PNS,  $E_{\text{rot}} \sim 10^{52}$  erg.

Bulk of radiation emitted during  
**bounce**, when quadrupole moment  
changes abruptly, producing a  
**burst of GW** for  $\sim 10$  ms with  
maximum amplitude of  $\sim 10^{-21}$  @  
10kpc.

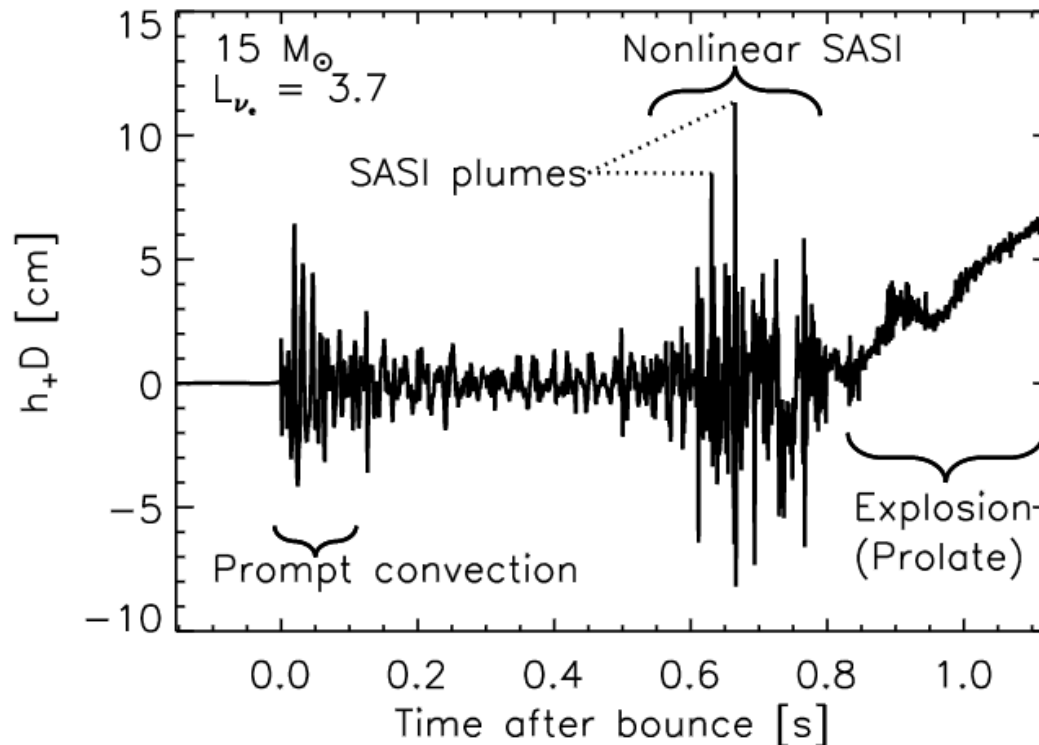
**Steep rise in amplitude** to positive  
values before bounce followed by a  
**negative peak** at bounce and a  
series of **damped oscillations**  
associated with the vibrations of the  
newly formed PNS. **Type I  
waveform.**

Dimmelmeier+ (2008)



# Post-bounce GWs: convection and SASI

After CC, hot PNS ( $10^{11}\text{K}$ ) cools down and shrinks to a compact NS, releasing  $\sim 3 \times 10^{53}$  erg as **neutrinos**. If a fraction of energy reabsorbed, it may heat up the post-shock region and lead to a successful SN explosion.

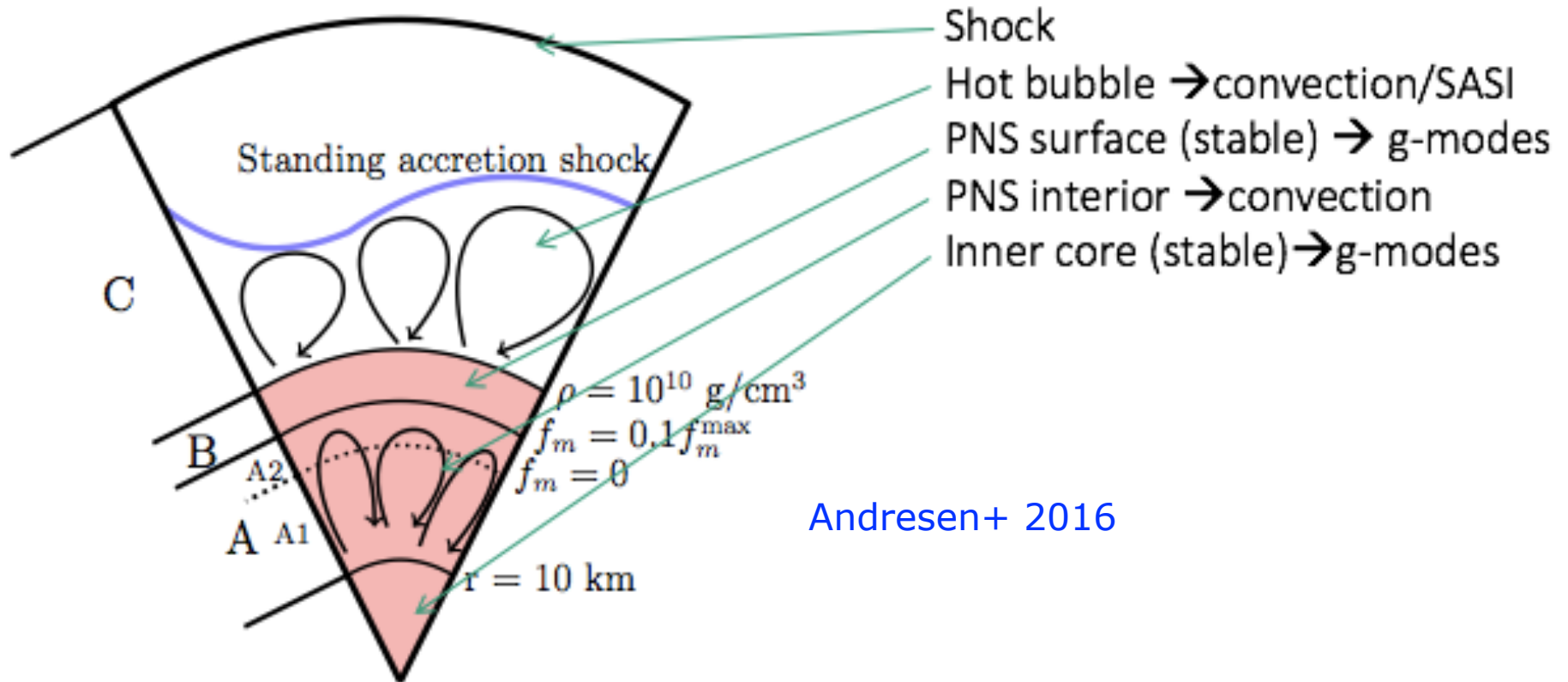


Murphy+ (2009)

**Stochastic signal.**  
Not straightforward  
to infer physics.

- prompt convection (negative entropy gradient left by stalling shock)
- PNS & post-shock convection
- SASI (spikes from narrow downflows striking the PNS "surface")
- explosion

# GW emission in CCSNe

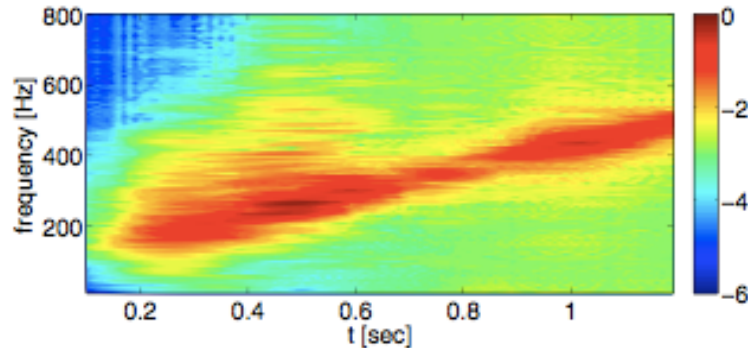


The most likely CCSN event is from a non-rotating progenitor (neutrino driven)

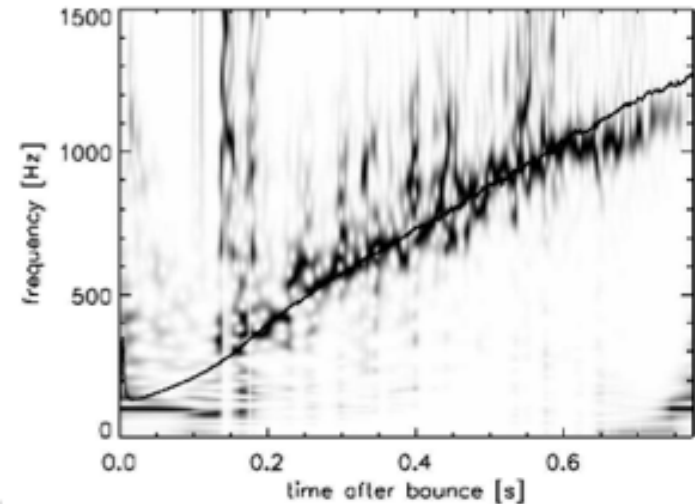
The proto-neutron star (PNS) is the source of most GW emission.

# Spectrograms

Arches with rising frequency associated with g-modes of PNS.



Müller+ 2012 (2D)

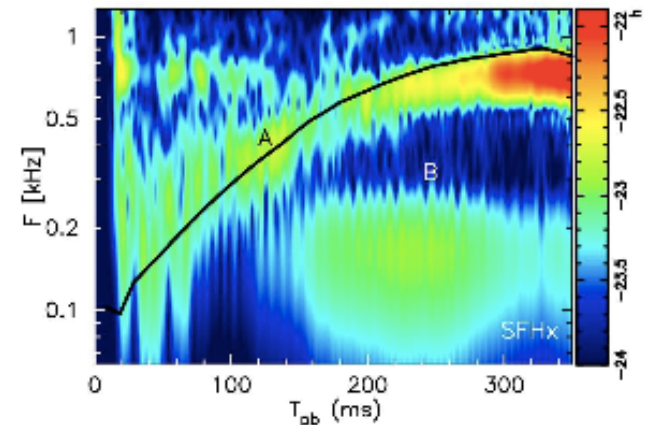


Müller+ 2013 (3D)

Features in GW spectra identified in previous works (Murphy+ 2009, Müller+ 2013). Frequencies raise monotonically with time due to the contraction of the PNS. Typical PNS frequencies as low as **100 Hz**, specially those related with **g-modes** (perfect target!)

If SASI present, additionally SASI modes.

Kuroda+ 2016



# CCSN asteroseismology

## Supernova modelling

- Sophisticated microphysics
- Computational challenges
- Progenitor uncertainties
- ...



Simulation  
templates

GW observations & data analysis

# CCSN asteroseismology

## Supernova modelling

- Sophisticated microphysics
- Computational challenges
- Progenitor uncertainties
- ...

## GW/mode frequency

- Surface gravity ( $M/R^2$ )
- Central density
- PNS surface temperature
- ...

GW observations & data analysis



Simulation templates  
+ mode analysis

Phenomenological  
parameterized  
templates

# Steps of our project

## 1. Identify properties of proto-neutron star

- Study of their normal modes of oscillation.
- Compare the mode spectrum with the frequencies of **gravitational-wave signals** from core-collapse simulations.

## 2. Find the relation with the physical parameter

- Perform numerical simulations.

## 3. Develop a model

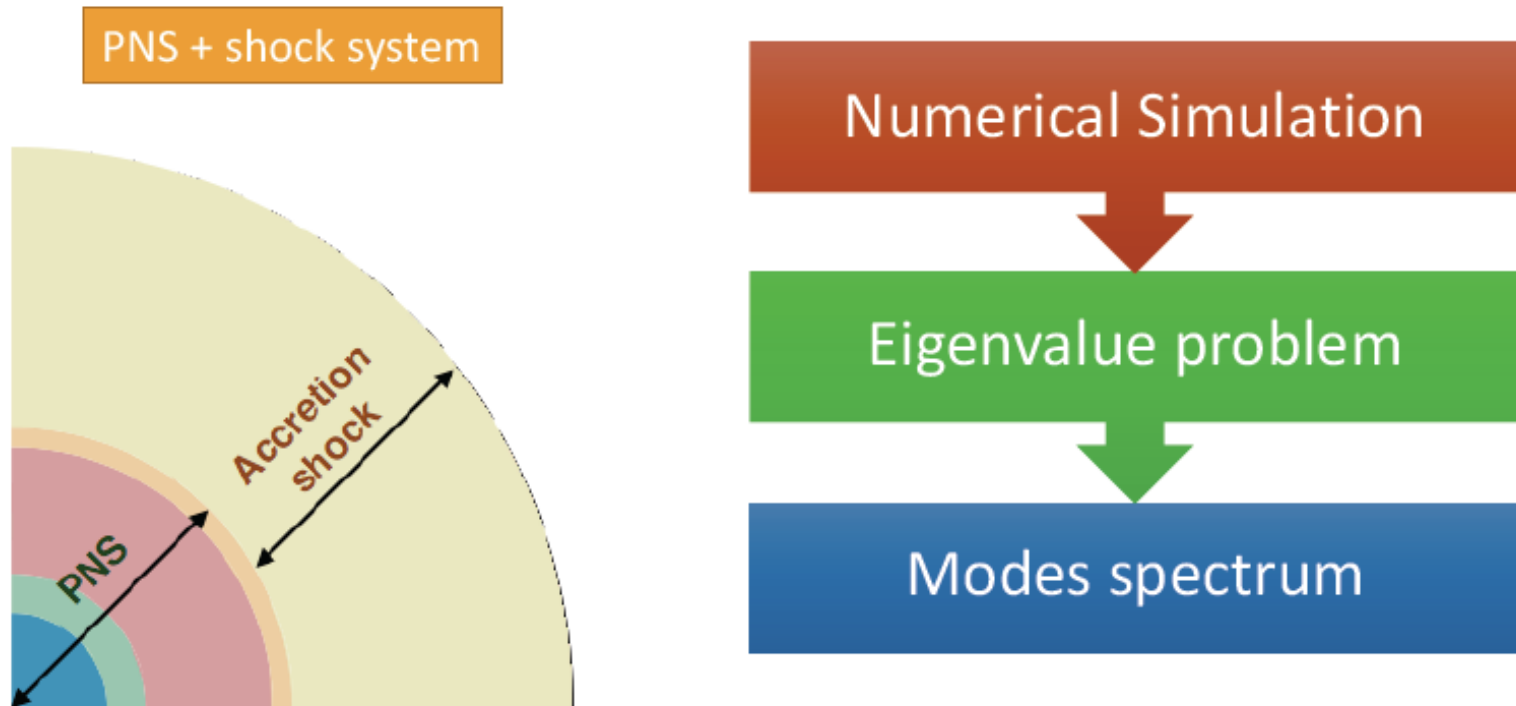
- Calculate a set of phenomenological templates.

## 4. Perform statistical parameter estimation

- Include the model and templates in standard codes.

# Currently at steps 1 and 2

Goal: check if it is possible to identify the properties of PNS based on the identification of mode frequencies in their waveforms.



System modeled as linear perturbations of spherical equilibrium background from CCSN numerical simulations (fluid + spacetime perturbations; [Torres-Forné+ 2018a,b](#), [Morozova+2018](#)).

# Our model in a nutshell

- Static, spherically-symmetric metric, isotropic coordinates

$$ds^2 = -\alpha^2 dt^2 + \psi^4 f_{ij} dx^i dx^j \quad \gamma_{ij} = \psi^4 f_{ij}$$

- EE in CFC + hydro equations (Valencia formulation)
- Static equilibrium solution of hydrodynamics+metric equations (unperturbed state or background solution)
- Linear adiabatic (Eulerian and Lagrangian) perturbations of the hydro+metric equations w.r.t. background solution

$$\rho \rightarrow \rho + \delta\rho \text{ (and so forth)} \quad \Delta\rho = \delta\rho + \xi^i \partial_i \rho$$

- Expansion of perturbations with harmonic time dependence and spherical-harmonic expansion for angular dependence

$$\text{e.g. } \delta P = \delta \hat{P} Y_{lm} e^{-i\sigma t} \quad \xi^\theta = \eta_\perp \frac{1}{r^2} \partial_\theta Y_{lm} e^{-i\sigma t}$$

- Impose boundary conditions at the shock location

# Fluid perturbations

$$\partial_r \eta_r + \left[ \frac{2}{r} + \frac{1}{\Gamma_1} \frac{\partial_r P}{P} + 6 \frac{\partial_r \psi}{\psi} \right] \eta_r + \frac{\psi^4}{\alpha^2 c_s^2} (\sigma^2 - \mathcal{L}^2) \eta_\perp = \frac{1}{c_s^2} \frac{\delta \hat{Q}}{Q} - \left( 6 + \frac{1}{c_s^2} \right) \frac{\delta \hat{\psi}}{\psi}$$

$$\partial_r \eta_\perp - \left( 1 - \frac{\mathcal{N}^2}{\sigma^2} \right) \eta_r + \left[ \partial_r \ln q - \mathcal{G} \left( 1 + \frac{1}{c_s^2} \right) \right] \eta_\perp = \frac{\alpha^2}{\psi^4 \sigma^2} \left[ \partial_r (\ln \rho h) - \left( 1 + \frac{1}{c_s^2} \right) \mathcal{G} \right] \left( \frac{\delta \hat{Q}}{Q} - \frac{\delta \hat{\psi}}{\psi} \right)$$

$\eta_r, \eta_\perp$  eigenfunctions: amplitudes of Lagrangian displacements

$\mathcal{N}, \mathcal{L}$  Brunt-Väisälä and Lamb frequencies

$$\mathcal{N}^2 = \frac{\alpha^2}{\psi^4} \mathcal{B} \mathcal{G} \qquad \mathcal{L}^2 \equiv \frac{\alpha^2}{\psi^4} c_s^2 \frac{l(l+1)}{r^2}$$

$\mathcal{G} = -\partial_r \ln \alpha$  gravitational acceleration

$$\mathcal{B} \equiv \mathcal{B}_r = \frac{\partial_r e}{\rho h} - \frac{1}{\Gamma_1} \frac{\partial_r P}{P} \qquad \text{Schwarzschild discriminant}$$

$\sigma$  frequency of harmonic time dependence

$$q \equiv \rho h \alpha^{-2} \psi^4$$

# Metric perturbations

$$\hat{\nabla}^2 \delta\hat{\psi} = -2\pi\psi^5 \left[ \left( 5e + \frac{\rho h}{c_s^2} \right) \frac{\delta\hat{\psi}}{\psi} - \frac{\rho h}{c_s^2} \frac{\delta\hat{Q}}{Q} \right] - 2\pi\rho h\psi^5 \left( \frac{\psi^4 \sigma^2}{\alpha^2 c_s^2} \eta_{\perp} - \mathcal{B}\eta_r \right)$$

$$\hat{\nabla}^2 \delta\hat{Q} = 2\pi(\rho h + 5P)\alpha\psi^5 \left( \frac{\delta\hat{Q}}{Q} + 4\frac{\delta\hat{\psi}}{\psi} \right) + 2\pi\rho h\alpha\psi^5 \left[ \left( 6 + \frac{1}{c_s^2} \right) \left( \frac{\psi^4 \sigma^2}{\alpha^2} \eta_{\perp} - \frac{\delta\hat{Q}}{Q} + \frac{\delta\hat{\psi}}{\psi} \right) - \eta_r \mathcal{B} \right]$$

$$\hat{\nabla}^2 \equiv \partial_{rr} + \frac{2}{r}\partial_r - \frac{l(l+1)}{r^2}$$

$$Q \equiv \alpha\psi$$

System of 6 first-order ODEs:

$$K \equiv \partial_r \delta\hat{Q}, \quad \Psi \equiv \partial_r \delta\hat{\psi}$$

$$\partial_r \mathbf{u} = \mathbf{A} \mathbf{u}$$

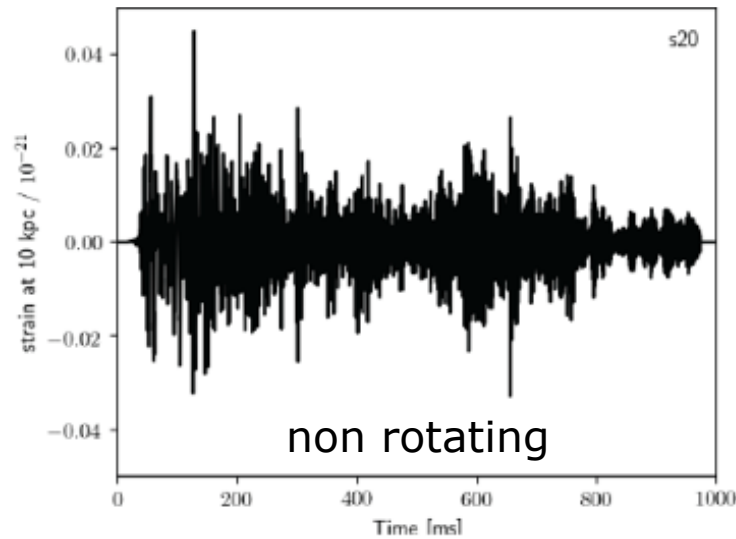
$$\mathbf{u} \equiv (\eta_r, \eta_{\perp}, K, \delta\hat{Q}, \Psi, \delta\hat{\psi})^T$$

## Procedure:

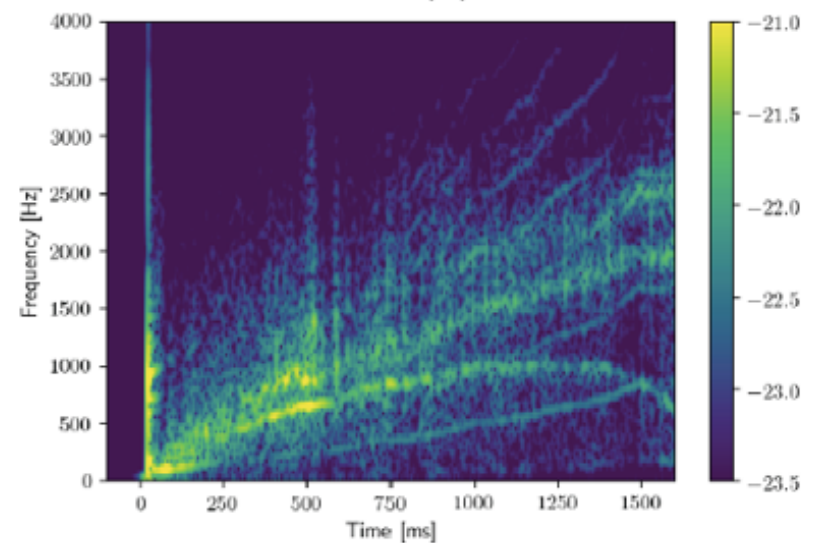
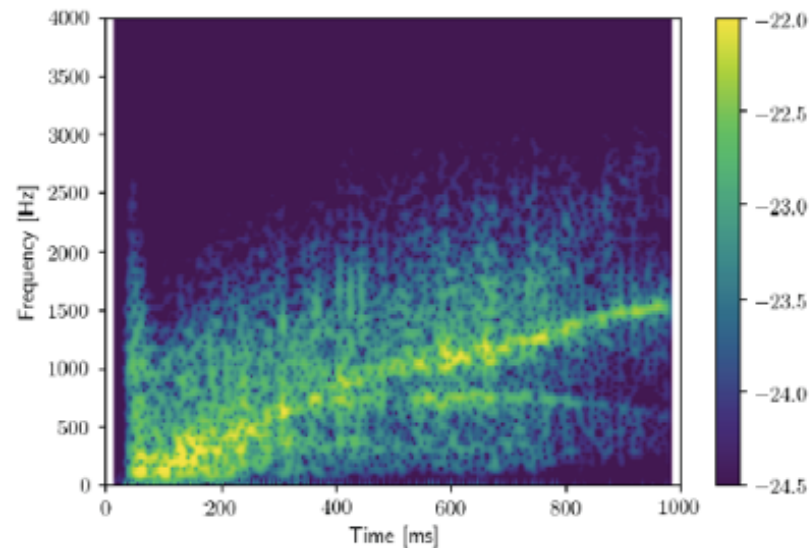
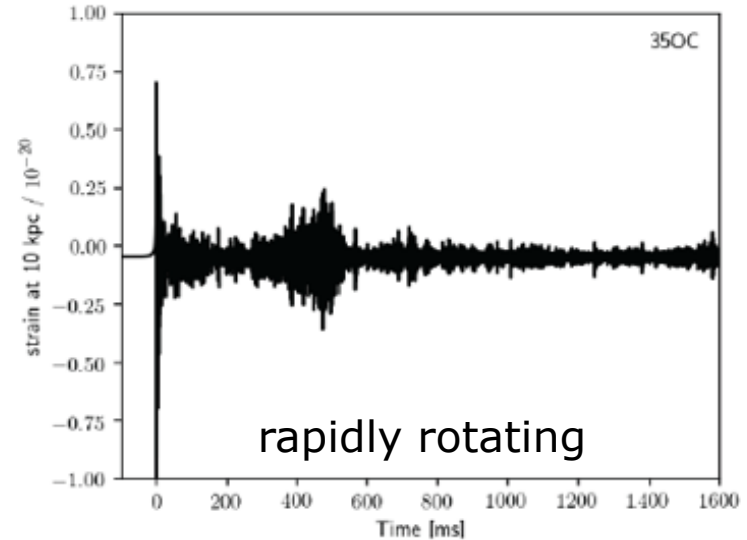
- 2D simulation with GW emission
- Angular averages to generate 1D profiles
- Linear analysis: calculation of eigenfrequencies and eigenfunctions
- Classification of eigenmodes: f/p/g modes
- Comparison with GW spectra from simulations (eventually from observations)

# Numerical simulations

Obergaulinger+ 2018

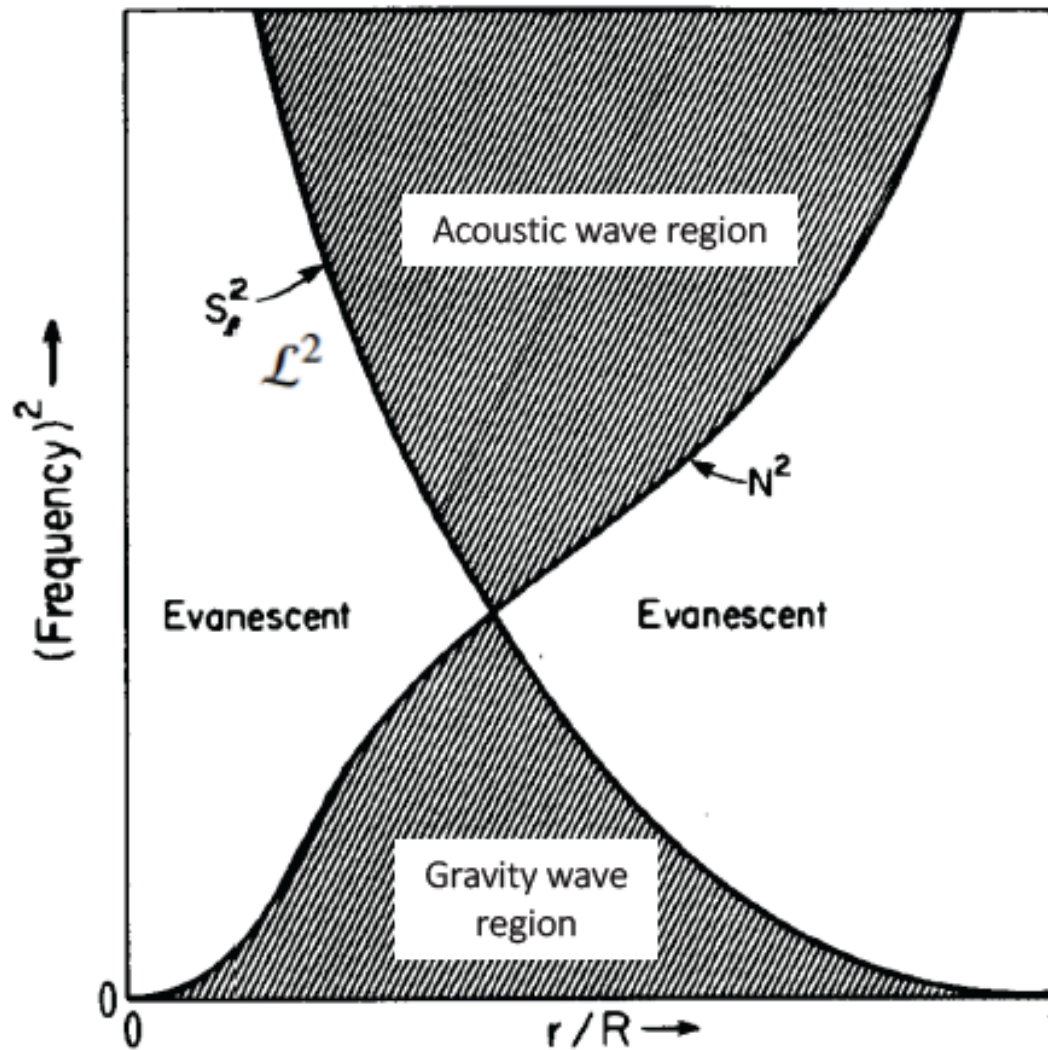


Cerdá-Durán+ 2013



Lines show frequency evolution of **p-** and **g-modes** at **PNS-shock cavity**.

# What are p/g/f-modes?



Stellar oscillations can be classified according to the dominant restoring force giving rise to them, either **pressure (p-modes)** or **buoyancy (g-modes)**.

The local quantities determining the character of the modes are the

$N^2$  : Brunt-Väisälä frequency

$\mathcal{L}^2$  : Lamb frequency

Acoustic wave region:

$$\sigma^2 > N^2, \mathcal{L}^2$$

Gravity wave region:

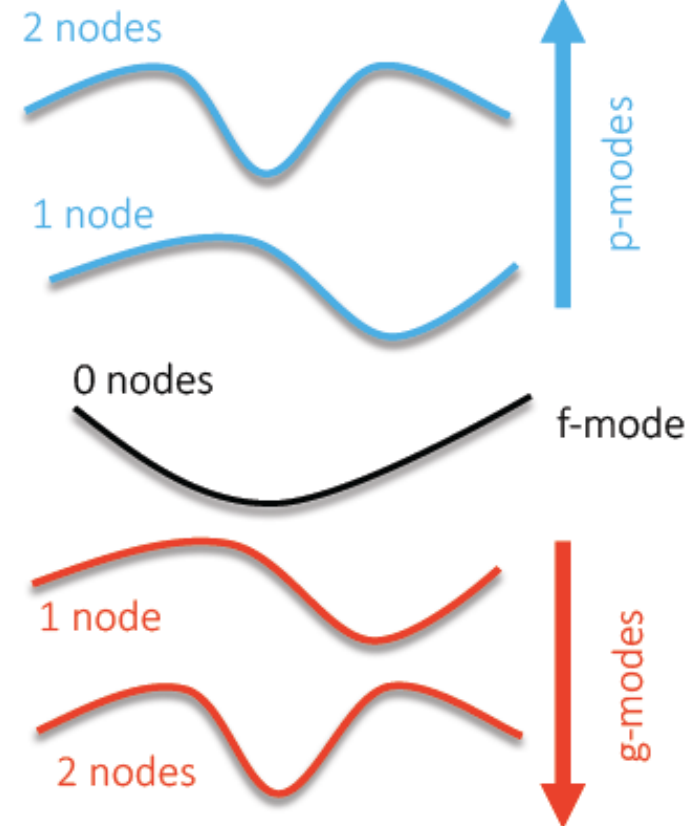
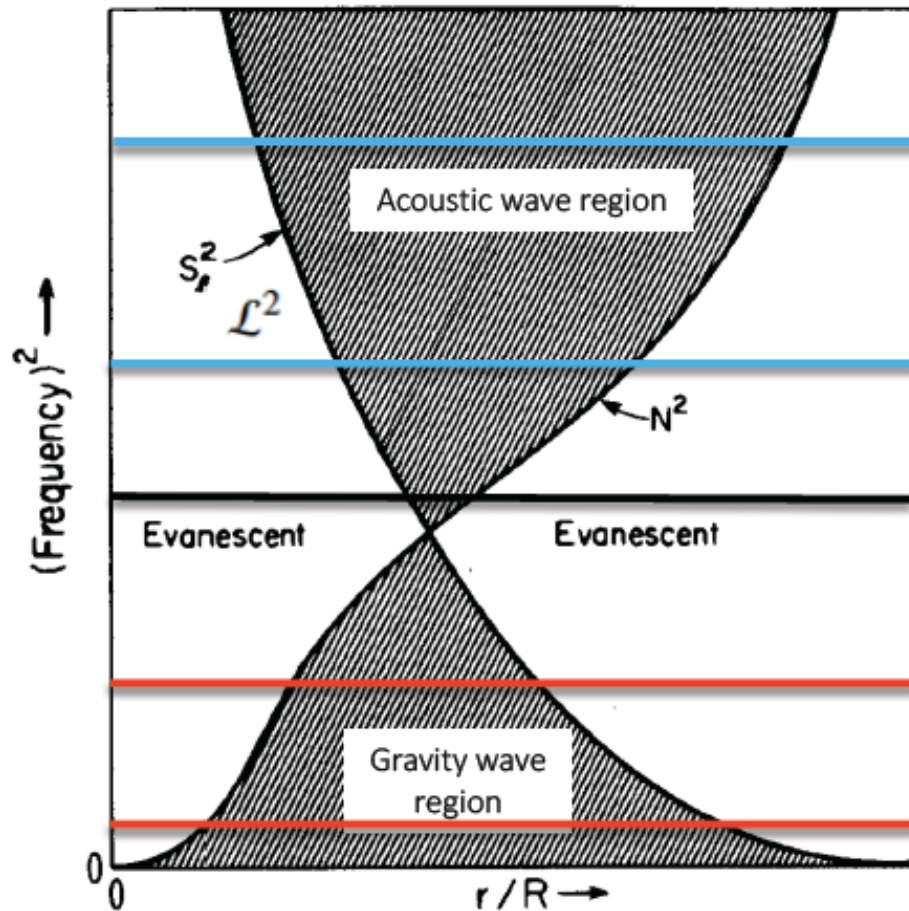
$$\sigma^2 < N^2, \mathcal{L}^2$$

← Propagation diagram

Cox 1980

# What are p/g/f-modes?

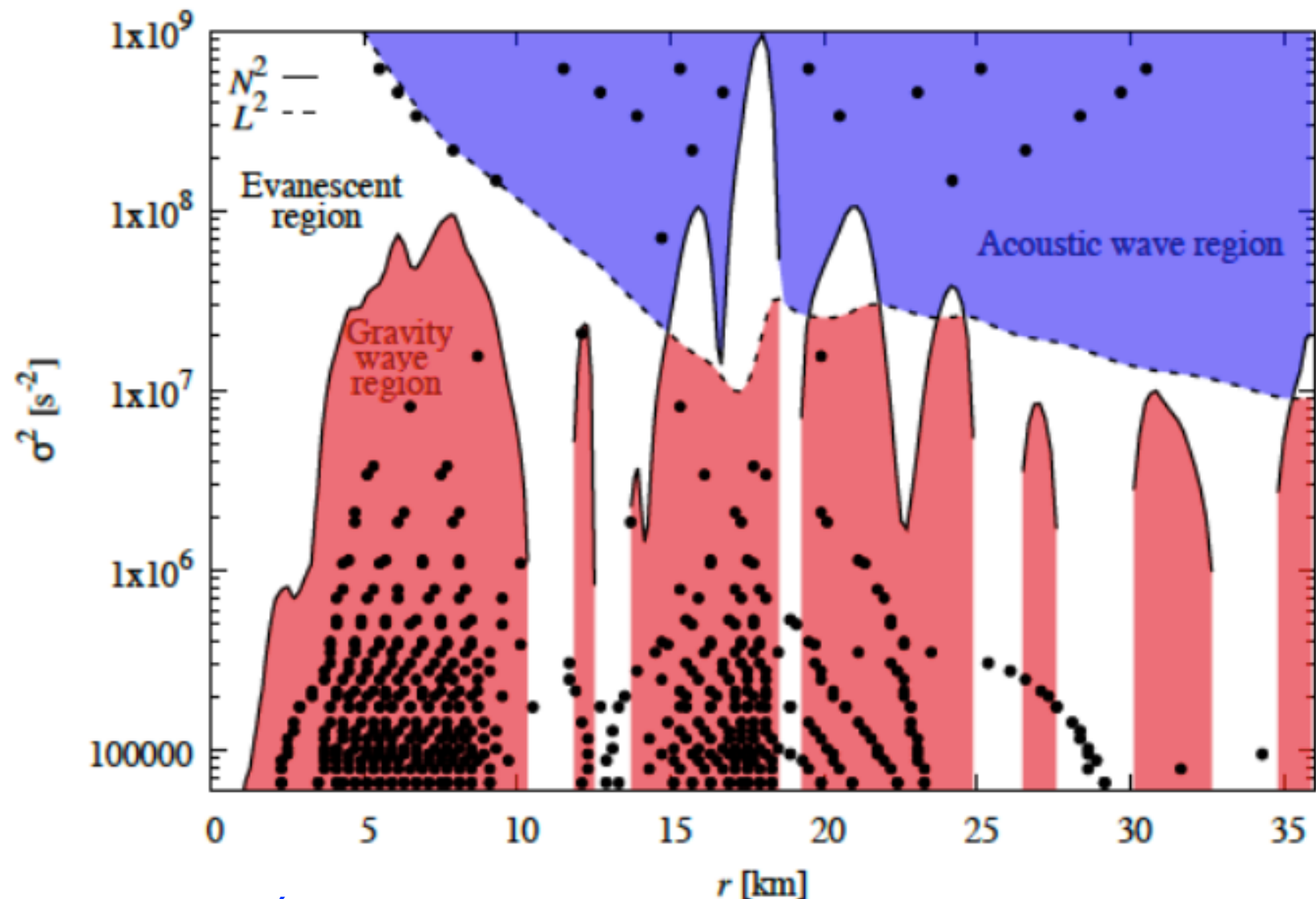
Cowling: simple classification purely based on the number of nodes of the radial part of the eigenfunction.



Cox 1980

Cowling 1941 classification

# p/g/f-modes in real life

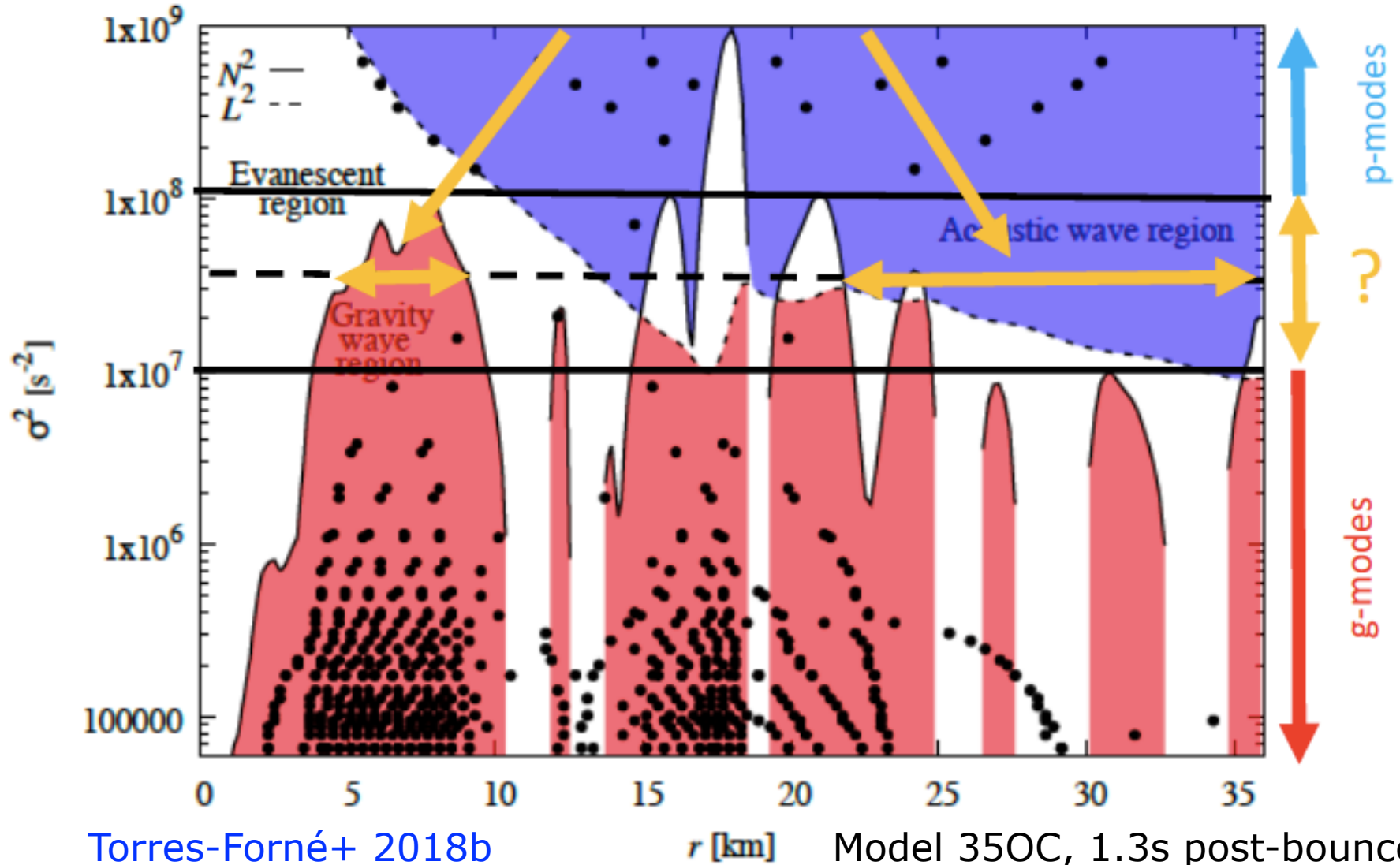


Torres-Forné+ 2018b

Model 350C, 1.3s post-bounce

# p/g/f-modes in real life

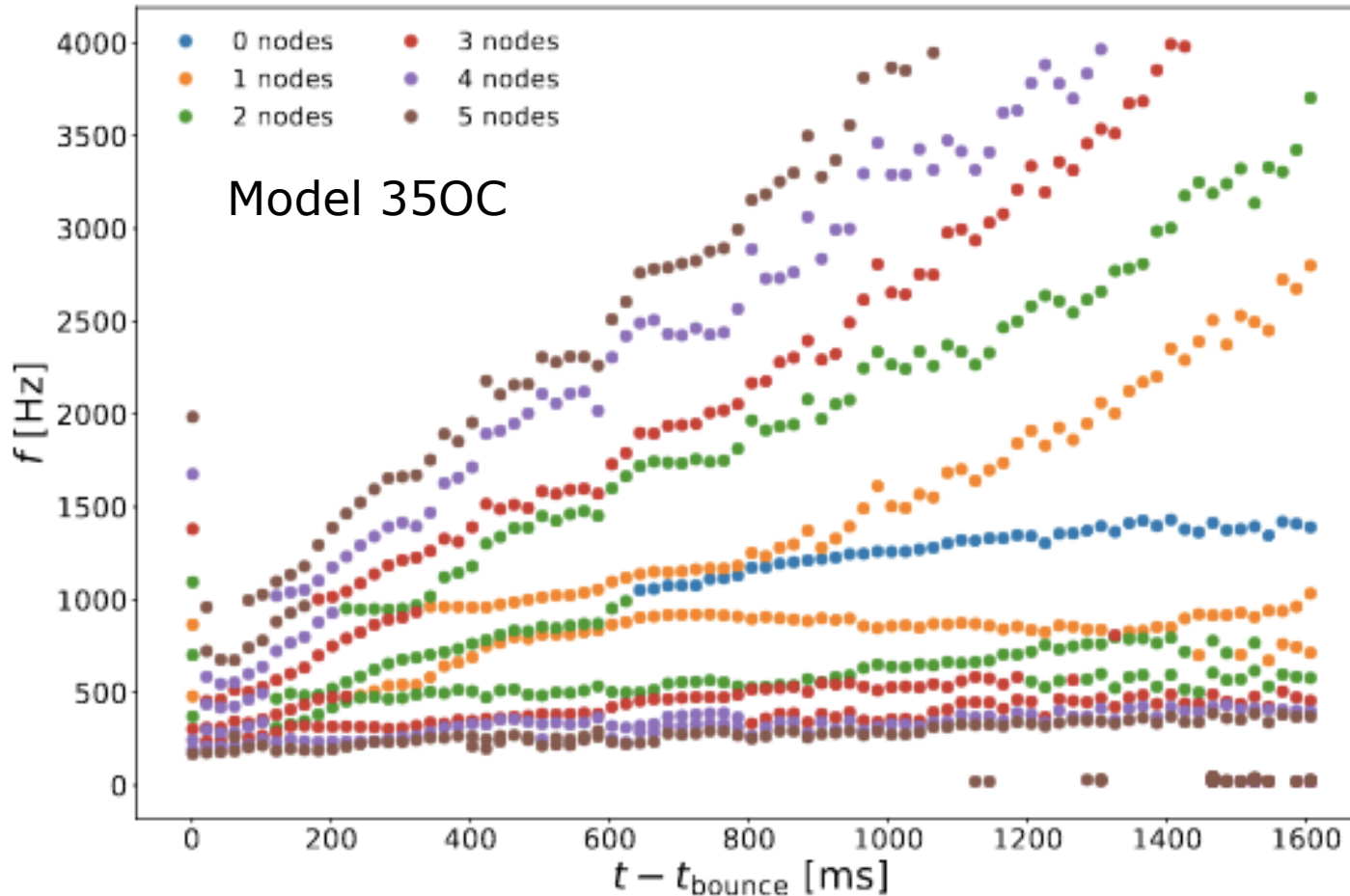
Trapped, interacting modes



# Mode classification: number of nodes

post-bounce evolution of mode frequencies

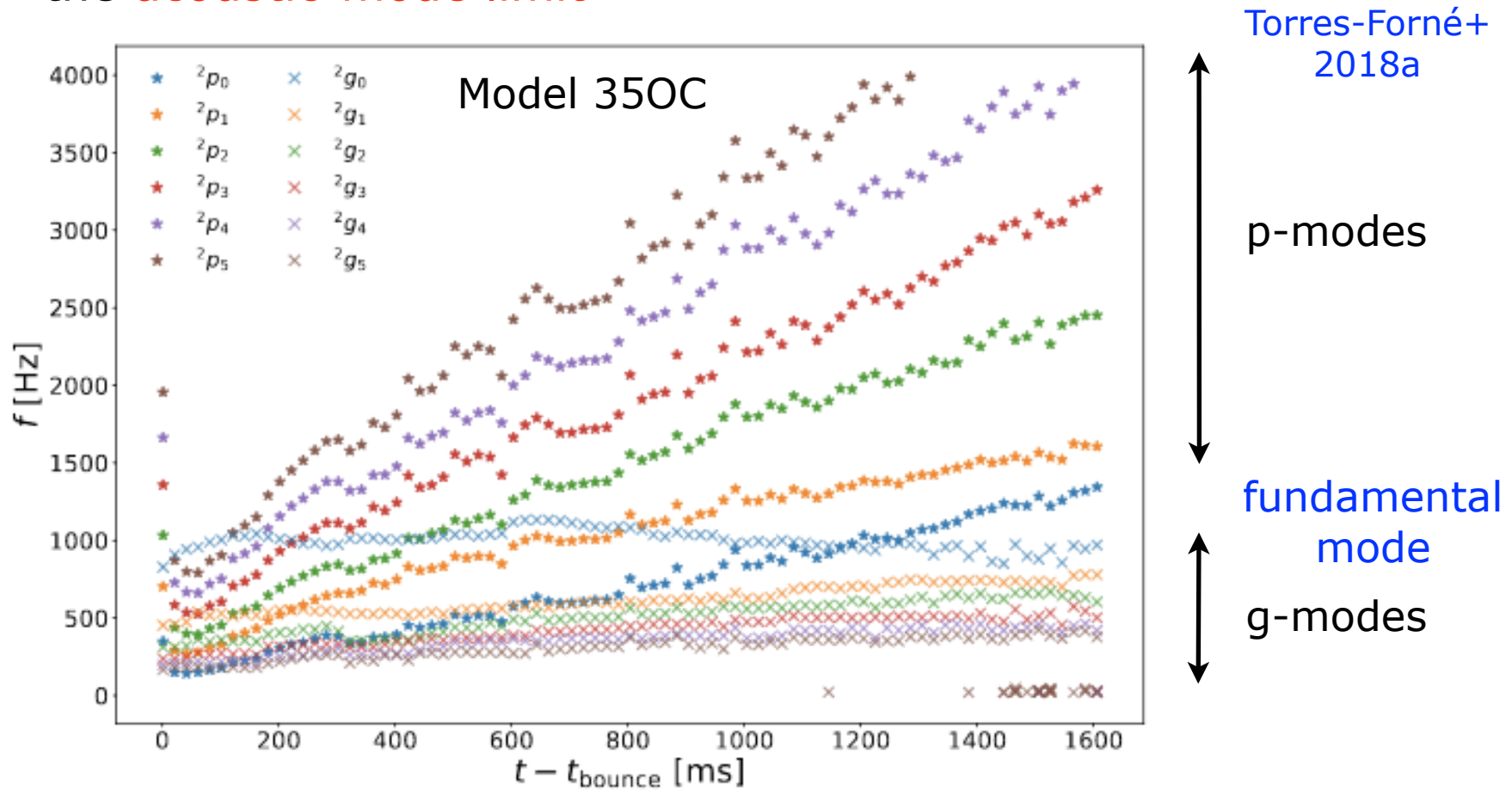
Torres-Forné+  
2018a



Theory says that # of nodes increases with increasing (decreasing) frequency for p-modes (g-modes)

# Mode classification: identification

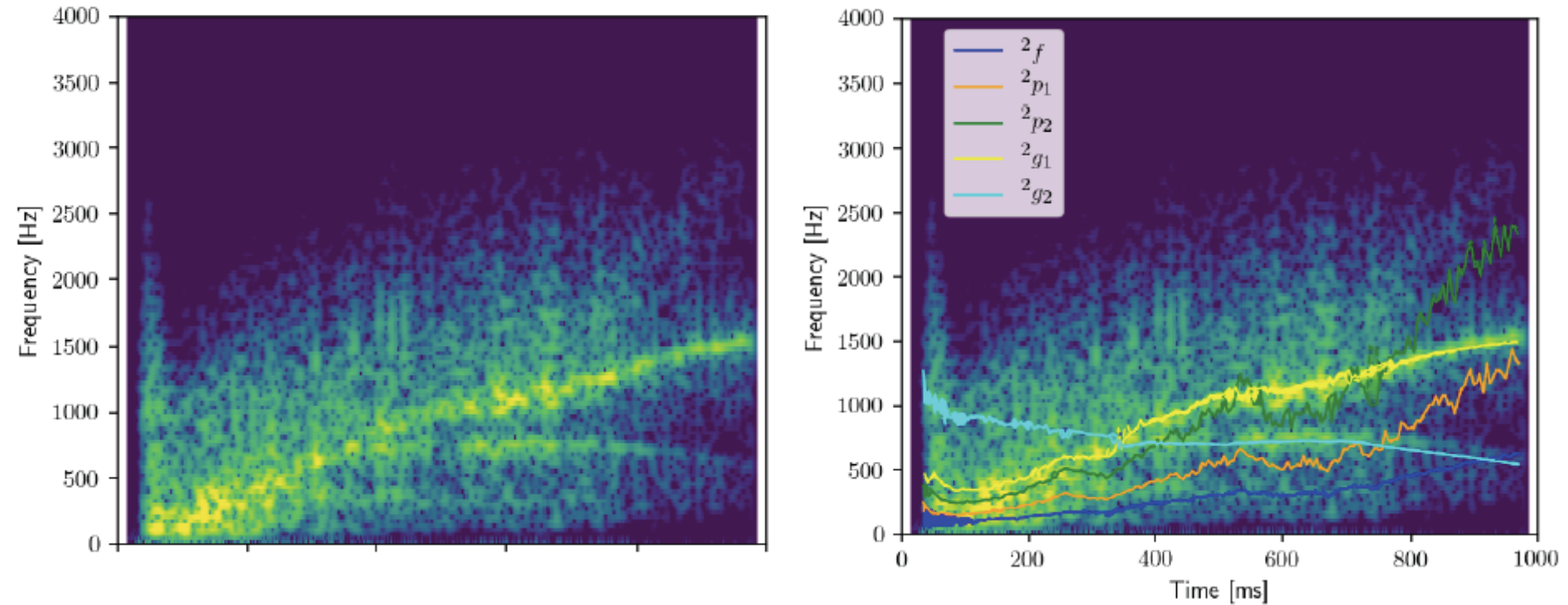
Approximate modes in the **buoyancy-mode limit** and in the **acoustic-mode limit**



**g-mode limit:**  $c_s^2 \rightarrow \infty$   
(remove acoustic waves)

**p-mode limit:**  $\mathcal{B} = 0 \rightarrow \mathcal{N}^2 = 0$   
(remove buoyancy)

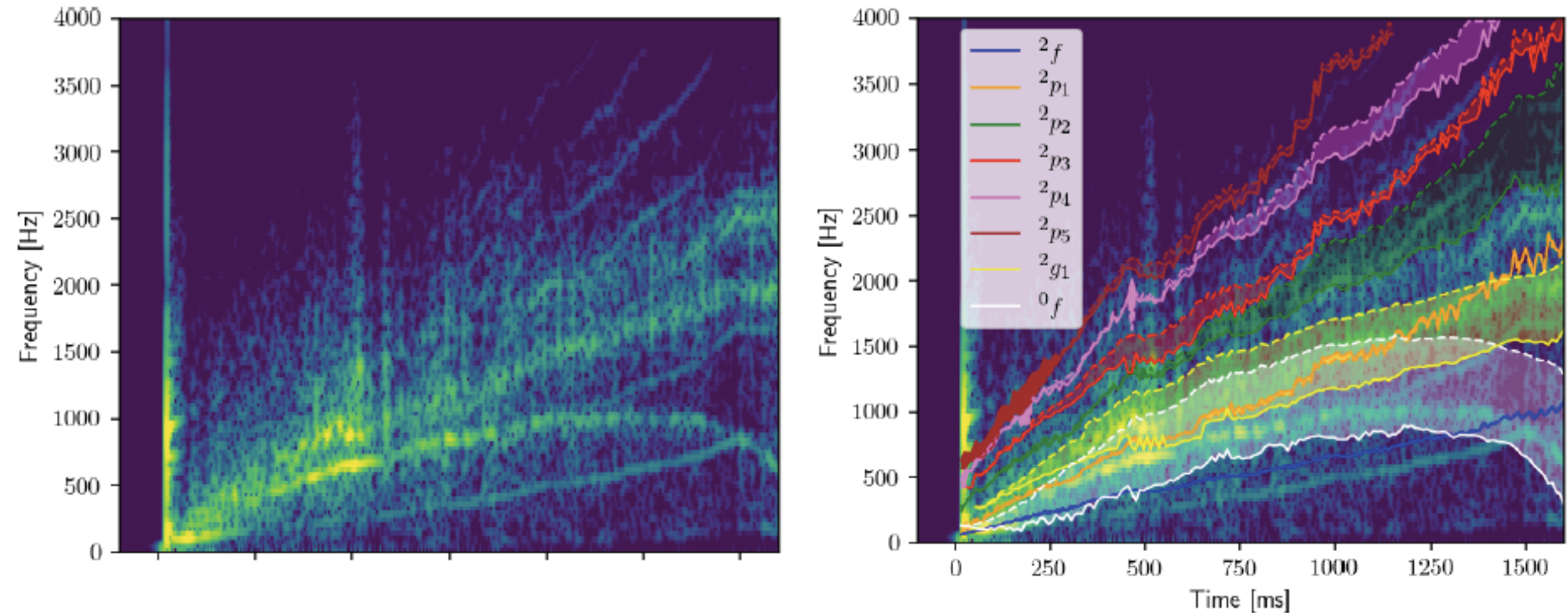
# Comparison with simulation - s20



## Lowest order modes are dominant.

- Lowest-order core g-mode ( ${}^2g_1$ ) is the dominant mode.
- ${}^2g_2$  also visible.
- Hints of the f-mode

# Comparison with simulation - 350C



350C is fast rotating (strong deformations)  
SASI develops during simulations

- Lowest-order core g-mode ( ${}^2g_1$ ) is the dominant mode.
- f and p-modes visible.
- Fundamental  $l=0$  mode visible.
- Uncertainties due to rotation.

# Asteroseismology of CCSNe

Let us suppose that we detect in the near future GWs from a CCSN event:

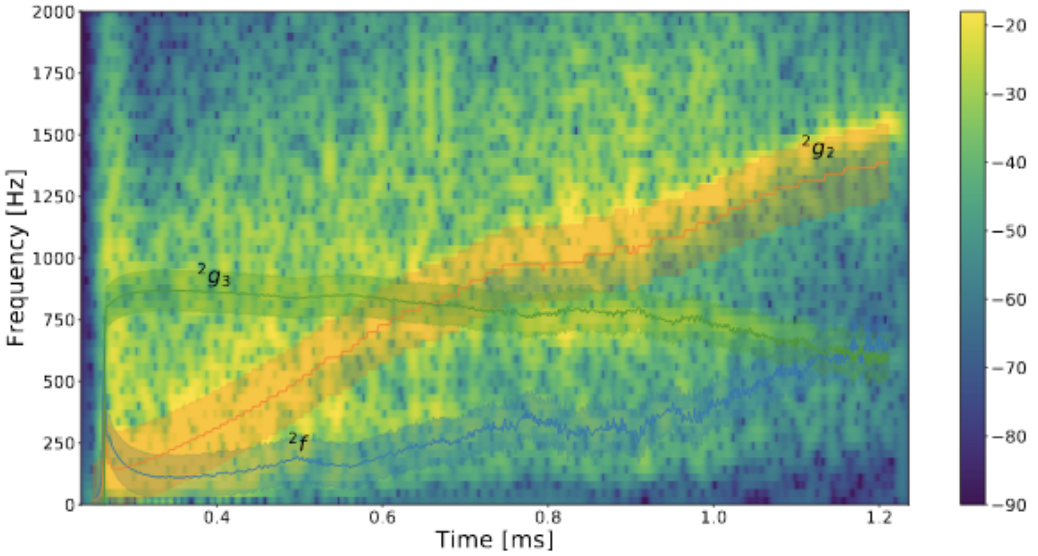
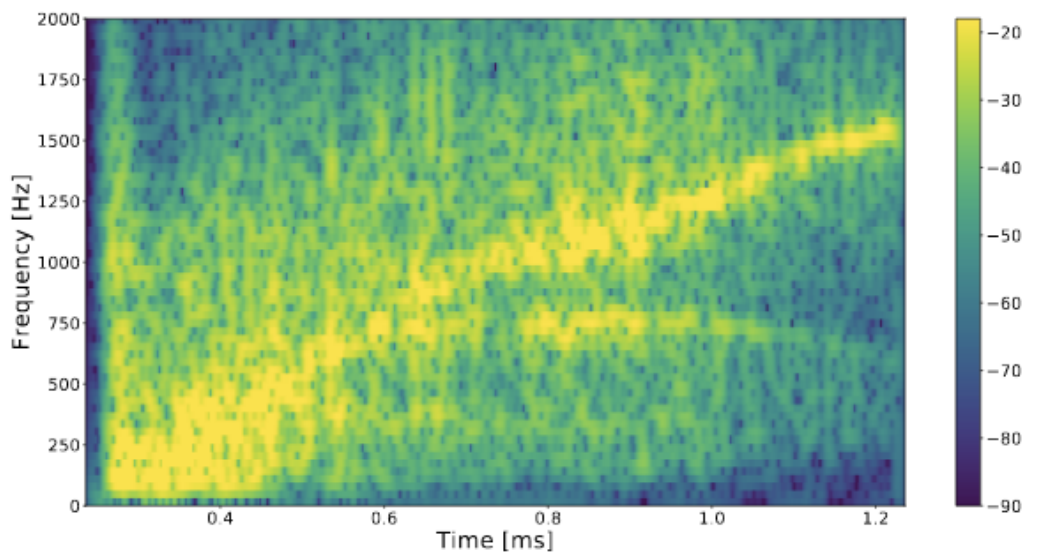
- What information can we extract from the measurement of the frequency evolution?
- Are there **universal relations** between PNS parameters and mode frequencies?

Goal: use fundamental relations for the **inverse problem**.

Can we measure  $M$  and  $R$  independently?  
(with detector noise)

# 1D simulations and mode identification

Code	Progenitor	EOS	Gravity
Aenus-ALCAR	s11.2	LS220	Newtonian
Aenus-ALCAR	s11.2	LS220	TOV-A
Aenus-ALCAR	s15	LS220	TOV-A
Aenus-ALCAR	s15	BHB-A	TOV-A
Aenus-ALCAR	s15	GShen-NL3	TOV-A
Aenus-ALCAR	s15	HShen	TOV-A
Aenus-ALCAR	s15	HShen- $\lambda$	TOV-A
Aenus-ALCAR	s15	SFHo	Newtonian
Aenus-ALCAR	s20	LS220	TOV-A
Aenus-ALCAR	s20	LS220	TOV-A
Aenus-ALCAR	s25	LS220	Newtonian
Aenus-ALCAR	s25	LS220	TOV-A
Aenus-ALCAR	s25	BHB-A	TOV-A
Aenus-ALCAR	s30	LS220	Newtonian
Aenus-ALCAR	s30	LS220	TOV-A
Aenus-ALCAR	s40	LS220	TOV-A
Aenus-ALCAR	s75	LS220	TOV-A
Aenus-ALCAR	u20	LS220	TOV-A
CoCoNuT	s11.1	LS220	XCFC
CoCoNuT	s15	LS220	XCFC
CoCoNuT	s20	LS220	XCFC
CoCoNuT	s25	LS220	XCFC
CoCoNuT	s30	LS220	XCFC
CoCoNuT	s40	LS220	XCFC
CoCoNuT	s75	LS220	XCFC



# Universal relations

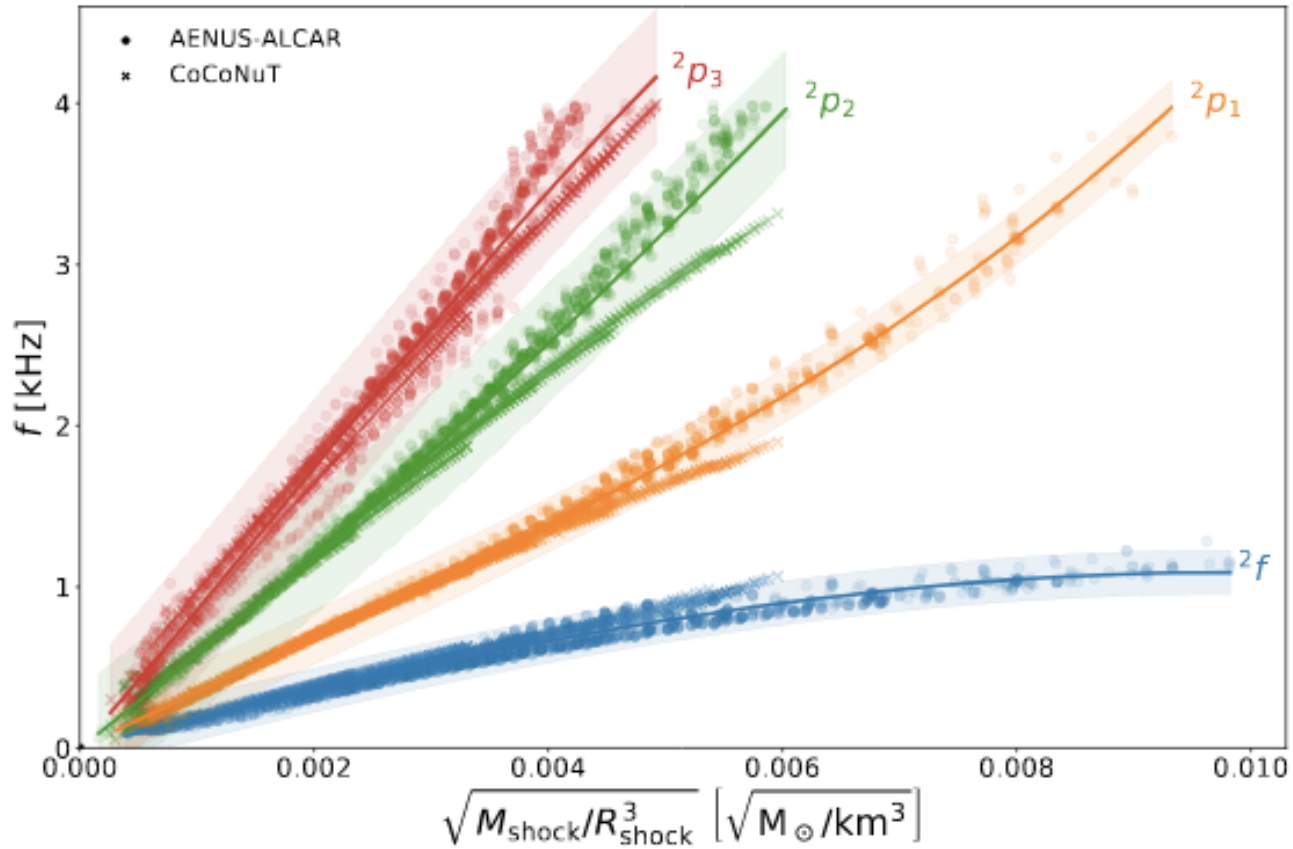
There exist **universal relations** that relate the frequencies of the most common oscillation modes observed, i.e. g-, p-and the f-mode, with fundamental properties of the system, (surface gravity of the PNS or mean density in the region enclosed by the shock).

$$f = a + bx + cx^2 + dx^3$$

mode	$x$	$a$	$b \times 10^5$	$c \times 10^6$	$d \times 10^{10}$	$R^2$	$\sigma$
${}^2f$	$\sqrt{M_{\text{shock}}/R_{\text{shock}}^3}$	-	$2.00 \pm 0.01$	$-8.5 \pm 0.1$	-	0.967	45
${}^2p_1$	$\sqrt{M_{\text{shock}}/R_{\text{shock}}^3}$	-	$3.12 \pm 0.01$	$9.3 \pm 0.2$	-	0.991	61
${}^2p_2$	$\sqrt{M_{\text{shock}}/R_{\text{shock}}^3}$	-	$5.68 \pm 0.03$	$14.7 \pm 0.7$	-	0.983	123
${}^2p_3$	$\sqrt{M_{\text{shock}}/R_{\text{shock}}^3}$	-	$8.78 \pm 0.04$	$-4 \pm 1$	-	0.979	142
${}^2g_1$	$M_{\text{pns}}/R_{\text{pns}}^2$	-	$18.3 \pm 0.05$	$-225 \pm 2$	-	0.982	140
${}^2g_2$	$M_{\text{pns}}/R_{\text{pns}}^2$	-	$12.4 \pm 0.01$	$-378 \pm 5$	$4.24 \pm 0.08$	0.967	76
${}^2g_3$	$\sqrt{M_{\text{shock}}/R_{\text{shock}}^3} \rho_C/\rho_C^{2.5}$	$905 \pm 3$	$-1.13 \pm 0.02$	$2.2 \pm 0.5$	-	0.925	41

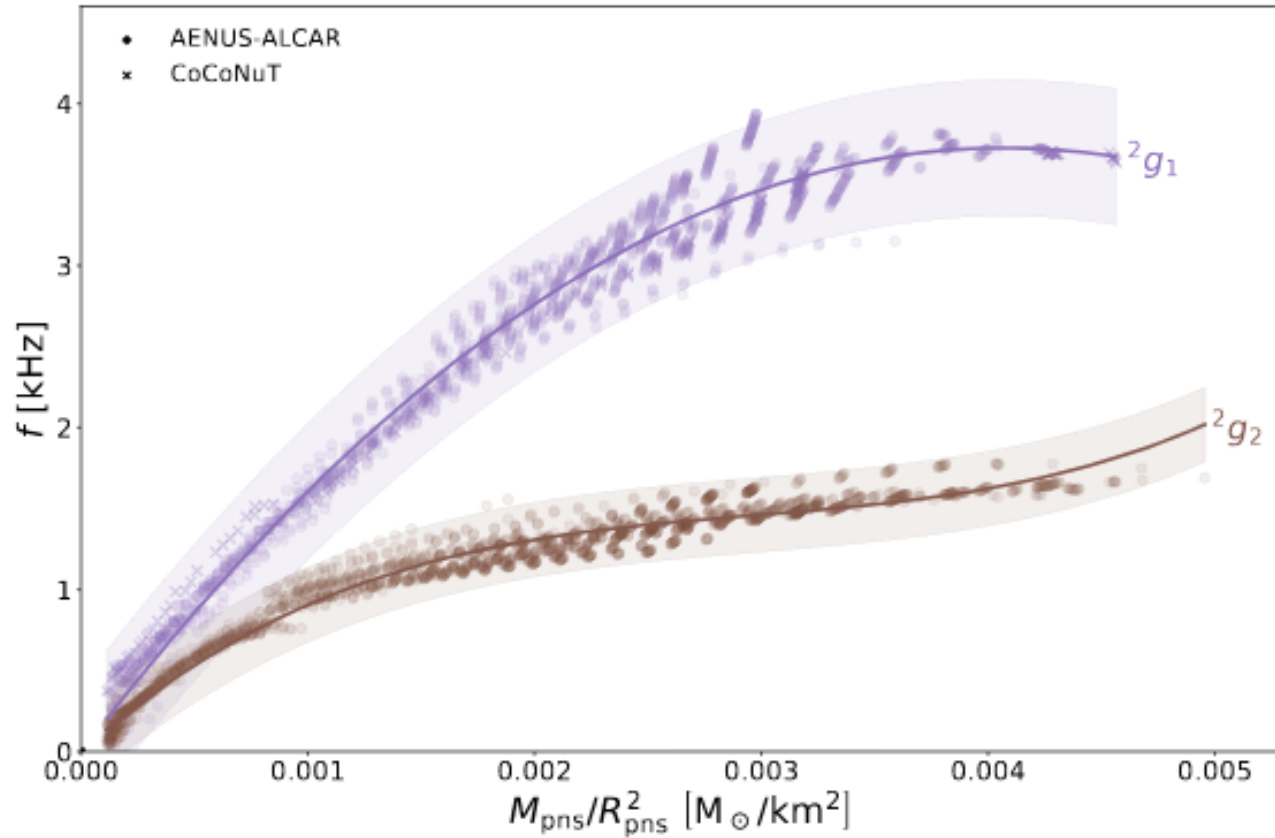
**Relations independent of EoS, neutrino treatment, and progenitor mass.** Hence, can be used to build methods to infer PNS properties from GW observations alone.

# Universal relations



f-mode and p-modes

# Universal relations



g-modes

# Summary and outlook

- GW observations of NS oscillations may soon become possible (Advanced LIGO/Virgo design sensitivity, 3G detectors). NS internal properties (radii, EOS, etc) may thus be inferred (as done for the Sun).
- **NS oscillations in HMNS from BNS mergers**
  - f-mode, combination frequencies and **inertial modes**.
  - Inertial modes triggered by a convective instability and their frequencies depend on the NS rotation rate: their detection in GWs could probe the rotational and thermal state of the merger remnant.
  - generality of result when including additional physics? (EOS with composition gradients, B-field, MRI, viscosity, neutrinos; important at  $t-t_m \sim 150$  ms and longer)
- **NS oscillations in PNS from CCSNe**
  - detectability? Low amplitude signal unless Galactic.
  - is it always the  ${}^2g_1$  mode the dominant mode in GW emission? 3D?
  - do universal relations hold for 2D/3D simulations?
  - additional physics